



HAL
open science

Combined Estimation of Material Law and Unloaded Configuration (Application to Pulmonary Poro-Mechanics)

Mahdi Manoochehrtayebi

► **To cite this version:**

Mahdi Manoochehrtayebi. Combined Estimation of Material Law and Unloaded Configuration (Application to Pulmonary Poro-Mechanics). Mechanical engineering [physics.class-ph]. 2020. hal-03043448

HAL Id: hal-03043448

<https://inria.hal.science/hal-03043448>

Submitted on 14 Jan 2021

HAL is a multi-disciplinary open access archive for the deposit and dissemination of scientific research documents, whether they are published or not. The documents may come from teaching and research institutions in France or abroad, or from public or private research centers.

L'archive ouverte pluridisciplinaire **HAL**, est destinée au dépôt et à la diffusion de documents scientifiques de niveau recherche, publiés ou non, émanant des établissements d'enseignement et de recherche français ou étrangers, des laboratoires publics ou privés.

MASTER THESIS

Combined Estimation of Material Law and Unloaded Configuration

Application to Pulmonary Poro-Mechanics

Author:
Mahdi MANOOCHEHRTAYEBI

Supervisor:
Martin GENET



Solid Mechanics Laboratory
ÉCOLE POLYTECHNIQUE (IP PARIS)

SEPTEMBER 2020

ABSTRACT

The human body acts as a complicated mechanical system. One of the subsystems in the human body is the respiratory system, which contains the lung and the thorax. Simulating this system as a mechanical system, mechanical properties, like stiffness for the lung, can be considered. Our lungs are under mechanical load by air. In the inhalation and exhalation process, the lung geometry passes through different configurations, but never the unloaded configuration. Finding this unloaded configuration is an interesting problem in biomechanics. In this paper, different mechanical systems have been studied, and methods for finding the unloaded configuration have been suggested, which are applied for solving such a problem for the lung. In this paper, it has been shown that estimating the unloaded configuration, one data point, which contains a loaded configuration and the corresponding applied force, is needed. and for material parameter estimation, if the dimension of the problem is more than the quantity of the material parameters, one data point is enough for material parameters estimation, too.

In this article, the inverse problem for the linear and nonlinear spring, Rivlin cube, tube, and at the end, the lung mechanical modeling has been discussed. The inverse problem is divided into the unloaded configuration and material parameter estimation. Methods used for solving the nonlinear equations are the gradient-free method, Newton nonlinear solver, and the gradient descent method. Moreover, the priority of the Newton solver has been shown.

The novelty studied in this project combines two classic problems in mechanics, and here the combined estimation of the material parameters and unloaded configuration has been discussed. In the end, the application of this estimation in lung pro mechanic has been studied. For modeling the lung mechanics, CT¹ (x-ray based) images during the inhalation and exhalation process for the hospital patients have been used.

¹Computed tomography

ACKNOWLEDGMENTS

Acknowledgments

Reaching to this peak of science, I was the smallest part of this power system, which pushed me here. First and foremost, all the honors and appreciations belong to my family, who tried more than me to reach up to here. I'm fortunate to have such a family and passed through a way in which I have become familiar with great people; each of them has played a role in my success.

In my master's internship period, it was time to start dealing with science, which is a very different way compared with what I was studying before. I am so grateful that I entered the science world under the supervision of Prof. Martin Genet, who made my mindset in the way of research, especially during this epidemic period in which I had to do almost all of my internship period at home; he was always accessible and in touch with me.

Besides Prof. Martin Genet, Cecile Patte has a significant portion of this project who shared her three-year Ph. D. research results and had much time training me. Many thanks to Dr. Taghvaeipour, Dr. Kamali, Prof. Michael Jabbour, Prof. Domonique Chapelle, École Polytechnique solid mechanics laboratory, Active M3DISIM team, and INRIA.

AUTHOR'S DECLARATION

I, Mahdi MANOOCHEHRTAYEBI, declare that this thesis titled, 'Combined Estimation of Material Law and Unloaded Configuration' and the work presented in it is my own. I confirm that this work submitted for assessment is my own and is expressed in my own words. Any uses made within it of other authors' works in any form (e.g., ideas, equations, figures, text, tables, programs) are appropriately acknowledged at any point of their use. A list of the references employed is included.

SIGNED: DATE:

TABLE OF CONTENTS

	Page
List of Figures	ix
1 Introduction	1
2 Combined Estimation of Material Parameters and Unloaded Configurations	7
2.1 Models	7
2.1.1 Linear Spring	7
2.1.2 Nonlinear Spring	8
2.1.3 Rivlin Cube	8
2.1.4 Tube	10
2.2 Forward Problem	11
2.2.1 A Method for Solving Nonlinear Problems	11
2.2.2 Linear Spring	12
2.2.3 Rivlin Cube	12
2.3 Inverse Problem	22
2.3.1 Methods for Minimizing a Cost Function	23
2.3.2 Methods for Computing Gradients and Hessians	24
2.3.3 Unloaded Configuration Estimation	29
2.3.4 Material Parameter Estimation	30
2.3.5 Combined Estimation of the Unloaded Configuration and Material Parameters	34
2.4 Finite Differences Approximation of the Derivative and Hessian Matrix	40
2.4.1 Computing the Gradient of Some Functions	40
3 Lung Mechanical Modeling	45
3.1 Introduction	45
3.1.1 Lung Mesh	45
3.1.2 Thorax Mesh	45
3.1.3 Lung Porosity	46
3.1.4 Thorax Displacement Field	46

TABLE OF CONTENTS

4 Discussion and Ongoing Research	51
Bibliography	53

LIST OF FIGURES

FIGURE	Page
1.1 Sketch of the general forward mechanical problem [12].	2
1.2 Illustration of Sellier’s iterative method for identifying a stress-free reference configuration in biomechanical boundary value problems [11].	2
1.3 Schematic of the reference configuration and the deformed configuration with the associated local quantities, volumes and porosity [9].	3
1.4 Kinematics of pre-strained biological systems. Pre-strain maps the stress-free reference configuration onto the residually stressed but mechanically unloaded configuration [3].	4
2.1 Minimization of the cost function of the nonlinear spring with respect to the material parameters	9
2.2 Tube geometry by Martin Genet in two different time steps under different loading pressures	10
2.3 The variation of Rivlin cube configuration and stress for the Saint Venant-Kirchhoff model under the applied axial compression in the x- direction	14
2.4 The variation of the Rivlin configuration and stress with respect to the equitriaxial pressure applied on the compressible Saint Venant-Kirchhoff model	14
2.5 The variation of Rivlin cube configuration and stress with respect to applied axial pressure for the compressible Mooney-Rivlin model	18
2.6 The variation of Rivlin cube configuration and stress with respect to applied equireiaxial pressure for the compressible Mooney-Rivlin model	18
2.7 The variation of Rivlin cube configuration and stress with respect to applied axial pressure for the incompressible Mooney-Rivlin model	19
2.8 The variation of Rivlin cube configuration and stress with respect to applied equireiaxial pressure for the incompressible Mooney-Rivlin model	19
2.9 Three different bulk energy models variation with respect to the compression index .	20
2.10 First derivative of three different bulk energy models variation with respect to the compression index	21

LIST OF FIGURES

2.11	Second derivative of three different bulk energy models variation with respect to the compression index	22
2.12	The variation of the pressure and displacement with respect to the lambda for the compressible Saint Venant-Kirchhoff model	30
2.13	Minimizing the cost function ($J(E)$) by CMA code for the linear spring.	31
2.14	The variation of λ in Saint-Venant Kirchhoff model with respect to the applied equitriaxial pressure applied on Rivlin Cube	32
2.15	The variation of Rivlin cube configuration and stress with respect to applied axial pressure for the incompressible Saint-Venant Kirchhoff model	32
2.16	The variation of Rivlin cube configuration and stress with respect to applied equitriaxial pressure for the incompressible Saint-Venant Kirchhoff model	33
2.17	Minimization of Mooney-Rivlin cube cost function with respect to re-scaled material parameters λ and μ	34
2.18	Minimization of Mooney-Rivlin cube cost function with respect to re-scaled material parameters λ and μ	35
2.19	Linear spring cost function minimization with respect to the re-scaled parameters of the unloaded configuration and Young modulus	37
2.20	Minimization of the cost of the linear spring with respect to two parameters of the unloaded configuration and stiffness coefficient	38
2.21	Minimization of Mooney-Rivlin cube cost function with respect to re-scaled material parameters λ and μ and unloaded configuration parameters.	38
2.22	Tube cost function minimization for the unloaded configuration and material parameter estimation via CMA code.	39
2.23	Tube cost function minimization for the unloaded configuration and material parameter estimation via Newton method.	39
2.24	Tube cost function minimization for the unloaded configuration and material parameter estimation via gradient descent method.	40
3.1	Lung surface mesh obtained in MeVisLab	46
3.2	Lung 3D mesh obtained in GMSH from the surface mesh	47
3.3	Lung CT images in three different angles	47
3.4	Thorax surface mesh obtained in MeVisLab	48
3.5	Thorax 3D mesh obtained in GMSH	48
3.6	CT image before and after porosity consideration	49
3.7	The right lung with different values of porosity. Blue color shows zero porosity and red color show parts with porosity equal to one.	49
3.8	Thorax mask images in three different angles	50
3.9	Thorax displacement field from end of the exhalation process and end of the inhalation process	50

INTRODUCTION

One classic problem in biomechanics is solving the inverse problem for a biomechanical system when the unloaded configuration or the material parameters are unknown. The new problem discussed here is the combined estimation of the unloaded configuration and material parameters. One of the exciting problems discussed in this paper will be developed later is to solve such a lung problem. This problem can be simulated to a mechanical system by finite element methods and considering a stiffness for it as a mechanical property where the controlling force is the air pressure.

In this chapter, some simple 1D to 3D problems have been discussed. In the end, the methods have been generalized for a more complicated problem like the tube, which has an n-dimensional configuration, making it more complicated to find a solution for the unloaded configuration.

The last model that has been discussed in this project is the lung poromechanic. The purpose of what has been discussed before is to model and find a lung poromechanics solution as the lung contains blood and air as the liquid in it. Besides the lung, the thorax plays an essential role in respiration, which is always in contact with the lung. So, thorax displacement can affect the inhalation and exhalation process.

Literature Review

For solving the inverse problem in hyperelasticity, different methods have been proposed. First of all, it is necessary to consider a re-parameterization of the weak form of the forward problem of finite elasticity as a solution method for the inverse incompressible problem. Many numerical approaches have been proposed for solving forward problems in incompressible finite elasticity. Most commonly, a mixed formulation is assumed with independent fields for displacements,

pressure, and sometimes the volumetric deformation[7].

The material used in this paper and cites govinde, *computational_1998* is the Neo-Hookean material with the

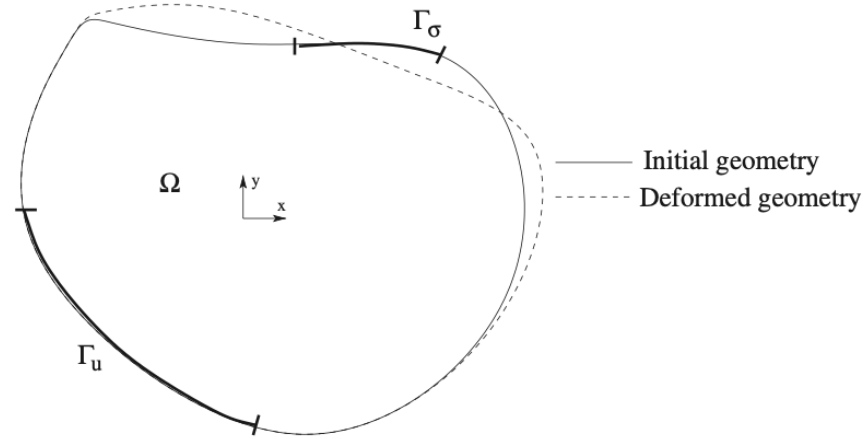


Figure 1.1: Sketch of the general forward mechanical problem [12].

The methods used in [12] has been implemented for a problem which contains fluid like what is discussed in the next chapter [11] as in Figure 1.2. The concept of the inverse problem in hyperelasticity is what is proposed in [2].

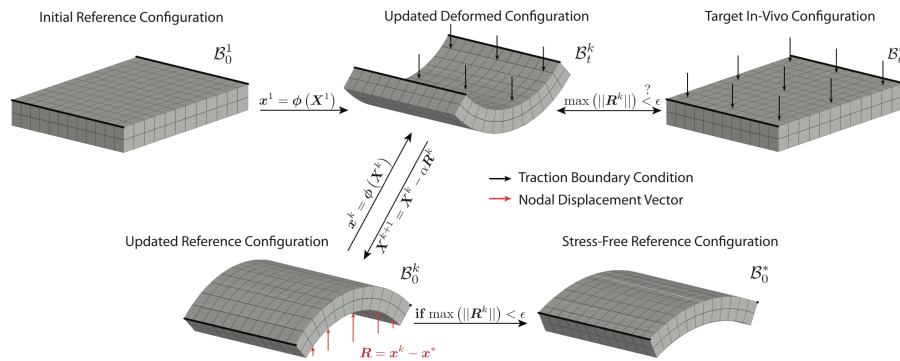


Figure 1.2: Illustration of Sellier's iterative method for identifying a stress-free reference configuration in biomechanical boundary value problems [11].

The concept of the inverse problem in hyperelasticity is what is proposed in [2].

As discussed in the last chapter, the inverse problem can be solved for the multi-dimensional problems if there are as many data points as needed. The same problem can be solved for the lung, but there are other aspects of this problem: the existence of the thorax and the porosity in the lung.

In [9], the lung's inverse problem by considering the porosity and poromechanics theory for large

deformations has been discussed hyperelastic potential reproducing the volumetric response of the pulmonary mixture to a change of pressure has been studied.

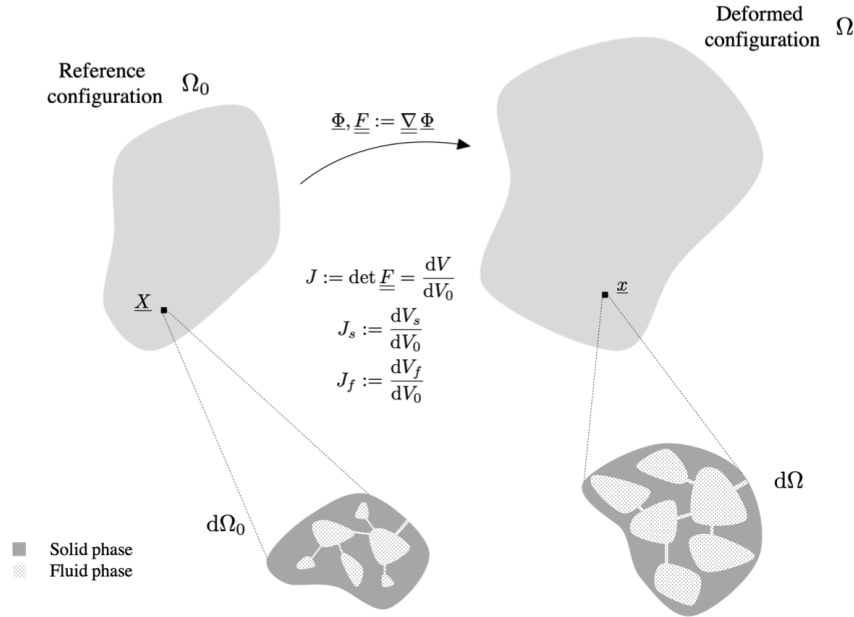


Figure 1.3: Schematic of the reference configuration and the deformed configuration with the associated local quantities, volumes and porosity [9].

A similar method has been discussed for the heart. The proposed method is embedded within the continuum theory of fictitious configurations and uses a fixed-point iteration on the geometry itself [3].

The motivation to work on the lung is its importance on human health as there are many pulmonary diseases. For example, a chronic disease in which collagen fibers accumulate into interstitial tissue leads to thickening, stiffening, and damage of alveolar walls. This disease remains poorly understood, poorly diagnosed, and poorly treated and represents a real clinical challenge. In interaction with data such as medical imaging, mechanical modeling-based tools could help clinicians in classifying patients and thus deciding on the treatment options [8]. For modeling the lung from the CT images, images registration tools have been implemented [4]. In the lung problem, the lung is in contact with the thorax, so the boundary problem by considering the contact between the lung and thorax should be considered in the boundary condition problem [10]. In [5], image processing has been implemented for the heart problem for extracting ventricular strain data from MR images.

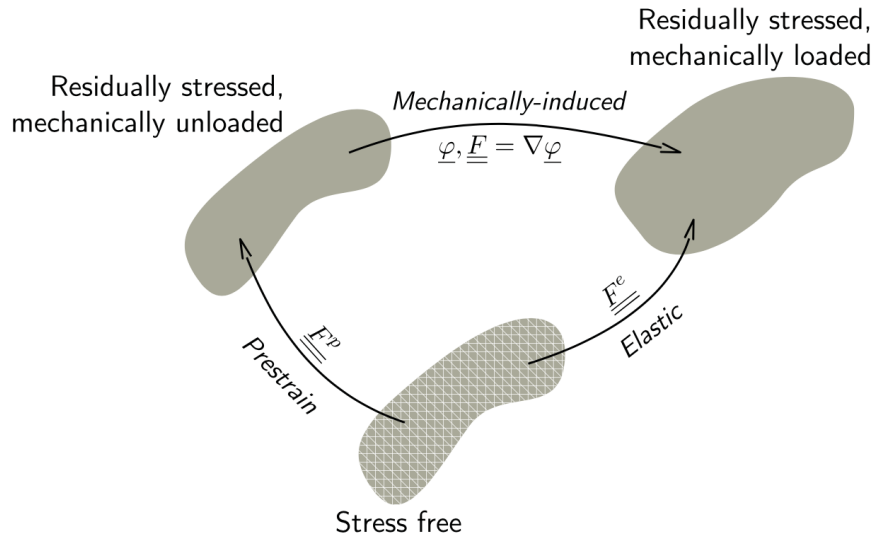


Figure 1.4: Kinematics of pre-strained biological systems. Pre-strain maps the stress-free reference configuration onto the residually stressed but mechanically unloaded configuration [3].

Types of the Problems Discussed

This chapter will start with the most simple problem, which is the linear spring. This problem has a one-dimensional configuration, which is the length of the spring. And also, there is stiffness for this spring as its material parameter.

Assumptions for obtaining the unknown material parameter and unloaded configuration is that the spring's length under an applied force has been measured. So, two applied forces with the corresponding deformed length are needed to obtain these two unknowns.

Different methods for solving this problem are implemented and generalized for a nonlinear spring and a three-dimensional problem, which is the Rivlin cube. For Rivlin cube, different material laws have been studied, and the more practical one is introduced. All the different methods have been implemented in the tube problem with the n -dimension configuration, and the more efficient one is introduced.

Materials and Methods

In mechanical systems, we may face problems in which the initial (unloaded) state is known, plus the material parameters. In this situation, the configuration under a specific load can be determined.

There are some unknown parameters, while these parameters like deformed configuration in these kinds of problems are known. Moreover, this deformed configuration is typically measured from the imaging data. So, there would be a cost function like Equation (1.1), which shows that

the parameter θ is the actual value when making the cost function minimum, which is equal to zero.

$$(1.1) \quad \theta = \operatorname{argmin} \left\{ J(\theta) = \frac{1}{2} \int_{\Omega^{mes}} (U(\theta) - U^{mes})^2 \right\}$$

So, the goal is to minimize the cost function, which varies from problem to problem. Nevertheless, the critical point is that the suggested cost function needs at least as many terms as the unknown parameters. There are different ways to minimize such a cost function, containing unknown parameters such as the material parameters or the unknown configurations. The unknown configuration depends on the problem dimension; for instance, it is one for a linear spring and three for a cube with three different dimensions.

COMBINED ESTIMATION OF MATERIAL PARAMETERS AND UNLOADED CONFIGURATIONS

Introduction

In this chapter, the inverse problem has been discussed for different models, and different methods have been implemented for solving the nonlinear equations. The inverse problem contains two aspects of the unloaded configuration and material parameter estimation, estimated together. Before going to the inverse problem concept, the forward problem has been explained. In the end, the minimization of the cost function has been discussed and methods of doing it.

2.1 Models

Materials discussed in this paper are linear and nonlinear spring, Rivlin cube, and a tube. Each of them has its material parameters and coordinates, which are discussed in the following.

2.1.1 Linear Spring

A linear spring is the most straightforward problem which can be discussed here. The linear spring has only a stiffness coefficient and a length, which changes by applying a force. In general, the linear spring law can be written as below:

$$(2.1) \quad E(u_{def} - u_{undef}) = F$$

E is the stiffness coefficient, F the applied force, and u_{undef} and u_{def} are the undeformed and deformed length, respectively.

2.1.2 Nonlinear Spring

For the linear spring, there was only one material parameter, which was the young modulus. For the nonlinear spring, there are two parameters for the nonlinear spring, which law is as mentioned below:

$$(2.2) \quad \sigma = E(\epsilon) \cdot \epsilon$$

$$(2.3) \quad E(\epsilon) = E_0 e^{\frac{\epsilon}{\epsilon_1}}$$

$$(2.4) \quad \sigma = E_0 e^{\frac{\epsilon}{\epsilon_1}} \cdot (\epsilon - \epsilon_0)$$

Three data points are needed for solving the inverse problem and material parameters for this geometry as there are two parameters as material parameters. The solving method is a bit different here, though the CMA¹ algorithm has been used again. For solving this problem with three data points and three unknown parameters, the solving process can be started from a known configuration with the applied force, different values for E_0 and ϵ_1 can be guessed, which are the material parameters.

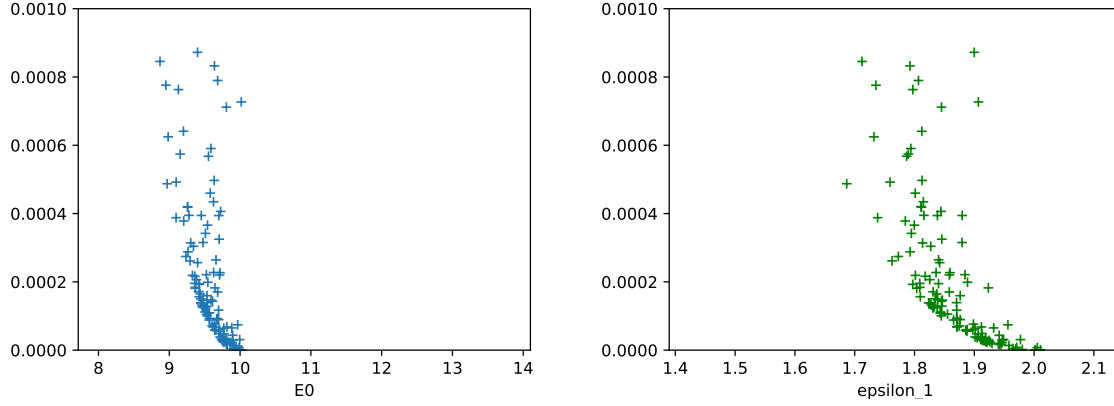
There are three deformed configurations with measured forces. So, the solving process can be started with one of the known configurations and with the guessed material parameters, and the unloaded configuration can be computed by it. There are an unloaded configuration and two measured forces with which two corresponding loaded configuration can be computed. Here, the cost function is defined as calculating the difference between the measured deformed configuration and the calculated ones. The minimization of the cost function concerning the material parameters are shown in the Figure 2.1

2.1.3 Rivlin Cube

What is mentioned simply for spring can be generalized for a 3D cube, which has three different dimensions, and any vector force can be applied on each aspect with different values that can deform the shape of the cube. If we applied force on a different aspect of such a cube, there would be deformation on each side. For example, if we apply forces on a cube with dimensions of:

$$(2.5) \quad \underline{X0} = \begin{bmatrix} x \\ y \\ z \end{bmatrix}$$

¹Covariance Matrix Adaptation



(a) Minimization of the cost function with respect to the material parameter E_0 (b) Minimization of the cost function with respect to the material parameter ϵ_1

Figure 2.1: Minimization of the cost function of the nonlinear spring with respect to the material parameters

After deforming such a cube under the force applied, the dimensions of the cube would be deformed as below:

$$(2.6) \quad \underline{X1} = \begin{bmatrix} \lambda_1 x \\ \lambda_2 y \\ \lambda_3 z \end{bmatrix}$$

Here we define matrix \underline{F} which is the deformation gradient.

$$(2.7) \quad \underline{F} = \begin{bmatrix} \lambda_1 & 0 & 0 \\ 0 & \lambda_2 & 0 \\ 0 & 0 & \lambda_3 \end{bmatrix}$$

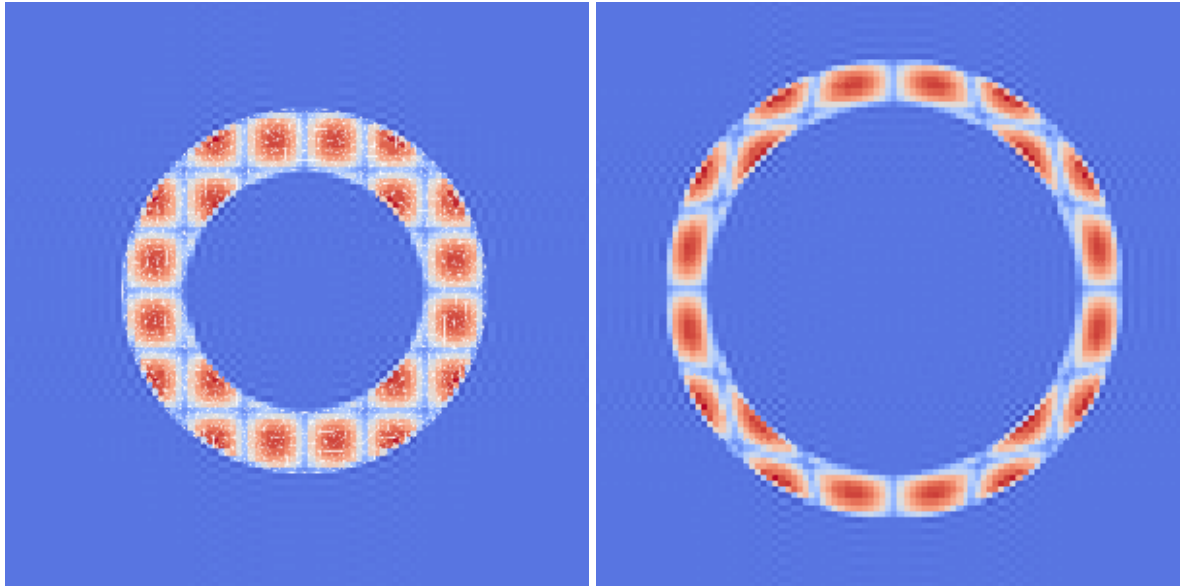
The right Green-Cauchy tensor \underline{C} and the left Green-Cauchy tensor \underline{b} are as below:

$$(2.8) \quad \underline{C} = \underline{F}^T \cdot \underline{F} = \begin{bmatrix} \lambda_1^2 & 0 & 0 \\ 0 & \lambda_2^2 & 0 \\ 0 & 0 & \lambda_3^2 \end{bmatrix}$$

$$(2.9) \quad \underline{b} = \underline{F} \cdot \underline{F}^T = \begin{bmatrix} \lambda_1^2 & 0 & 0 \\ 0 & \lambda_2^2 & 0 \\ 0 & 0 & \lambda_3^2 \end{bmatrix}$$

And \underline{E} is the Green-Lagrange strain tensor.

$$(2.10) \quad \underline{E} = \frac{\underline{C} - \underline{I}}{2} = \begin{bmatrix} \frac{\lambda_1^2 - 1}{2} & 0 & 0 \\ 0 & \frac{\lambda_2^2 - 1}{2} & 0 \\ Sym & & \frac{\lambda_3^2 - 1}{2} \end{bmatrix}$$



(a) Unloaded configuration of the tube

(b) Loaded configuration of the tube

Figure 2.2: Tube geometry by Martin Genet in two different time steps under different loading pressures

In which " $\underline{\underline{I}}$ " is the identity tensor:

$$(2.11) \quad \underline{\underline{I}} = \begin{bmatrix} 1 & 0 & 0 \\ 0 & 1 & 0 \\ 0 & 0 & 1 \end{bmatrix}$$

It is evident that the stress tensor is obtained from the derivative of the energy form. So, what we choose as our energy model can change the stress tensor.

2.1.4 Tube

Here a 2D tube has been discussed, which has an inner radius and an outer radius. This problem is symmetric and has a constant young modulus. The input of the problem is the tube inner pressure, which makes inflation of the tube.

This 2D problem is multi-dimensional in that it would be parameterized by the finite element method, and the node displacements would be the configuration of the problem. There is the young modulus as the material parameter for the tube problem and the unloaded configuration. There are some time steps, which are the configurations of the tube for different values of the inner pressure. In Figure 2.2, the first and last loaded configuration has been shown.

2.2 Forward Problem

This kind of problem is not very common to solve. The meaning of the forward problem is that we change the model configuration and see what forces correspond to the new configuration. In the real problem, this is rarely happening, or it may only be calculated to see the force needed to obtain the ideal configuration. In the following, the forward problem is demonstrated for the models discussed in this paper.

2.2.1 A Method for Solving Nonlinear Problems

For the hyperelastic model the stress tensor $\underline{\underline{\sigma}}(\underline{\lambda})$ should be equal to the applied pressure \underline{P} , but as an initial guess like $\underline{\lambda}_0$ we have a residual which is the difference between the stress tensor and the applied pressure vector:

$$(2.12) \quad \underline{R}_0 = \underline{\underline{\sigma}}(\underline{\lambda}_0) - \underline{P}$$

In the above equation, $\underline{\underline{\sigma}}$ and \underline{P} are defined as below:

$$(2.13) \quad \underline{\underline{\sigma}} = \begin{bmatrix} \sigma_{11} \\ \sigma_{22} \\ \sigma_{33} \end{bmatrix}$$

$$(2.14) \quad \underline{P} = \begin{bmatrix} P_1 \\ P_2 \\ P_3 \end{bmatrix}$$

And:

$$(2.15) \quad \underline{R}_0 = \begin{bmatrix} \sigma_{11} - P_1 \\ \sigma_{22} - P_2 \\ \sigma_{33} - P_3 \end{bmatrix}$$

Using Taylor expansion around λ_0 , we can obtain the update law.

$$(2.16) \quad \underline{\underline{\sigma}}(\underline{\lambda}_0 + \underline{\Delta\lambda}) \approx \underline{\underline{\sigma}}(\underline{\lambda}_0) + \frac{\partial \underline{\underline{\sigma}}}{\partial \underline{\lambda}}(\underline{\lambda}_0) \cdot \underline{\Delta\lambda}$$

As there is:

$$(2.17) \quad \underline{\underline{\sigma}}(\underline{\lambda}_0 + \underline{\Delta\lambda}) = \underline{P}$$

So, the update law would be like Equation (2.90)

$$(2.18) \quad \underline{\Delta\lambda}_0 = \frac{\underline{P} - \underline{\underline{\sigma}}(\underline{\lambda}_0)}{\frac{\partial \underline{\underline{\sigma}}}{\partial \underline{\lambda}}(\underline{\lambda}_0)} = -\underline{\underline{Jac}}^{-1} \cdot \underline{R}_0$$

In which $J_{\alpha c}$ is Jacobian matrix of σ :

$$(2.19) \quad \underline{\underline{J_{\alpha c}}} = \frac{\partial \underline{\underline{\sigma}}}{\partial \lambda}$$

What has been done here is that the cost function should be minimized, which means that its gradient should become zero. So, the newton method has been done on the derivative of the cost function.

2.2.2 Linear Spring

For a linear spring, The forward problem is such that the stiffness coefficient, applied force, and the undeformed length is known, and the only unknown is the deformed length, which can be obtained by the following relation:

$$(2.20) \quad u^{def} = u^{undef} + \frac{F}{E}$$

2.2.3 Rivlin Cube

What is mentioned simply for spring can be generalized for a 3D cube, which has three different dimensions, and any force vector can be applied on each face with different values that can deform the shape of the cube. If a force is applied to different aspects of such a cube, there would be deformation on each side. For example, the mentioned force can be applied on a cube by following dimensions:

$$(2.21) \quad \underline{\underline{X0}} = \begin{bmatrix} x \\ y \\ z \end{bmatrix}$$

After deformation of such a cube under the force applied, the dimensions of the cube would be deformed as below:

$$(2.22) \quad \underline{\underline{X1}} = \begin{bmatrix} \lambda_1 x \\ \lambda_2 y \\ \lambda_3 z \end{bmatrix}$$

Here matrix F which is the deformation gradient can be defined as below:

$$(2.23) \quad \underline{\underline{F}} = \begin{bmatrix} \lambda_1 & 0 & 0 \\ 0 & \lambda_2 & 0 \\ 0 & 0 & \lambda_3 \end{bmatrix}$$

2.2.3.1 Saint Venant-Kirchhoff Model

Saint Venant-Kirchhoff energy model is like the (Equation (2.24))

$$(2.24) \quad \Psi = \frac{\lambda}{2} (\text{tr} \underline{\underline{E}})^2 + \mu (\text{tr} \underline{\underline{E}}^2)$$

Stress tensor for compressible material can be obtain by derivative of the energy function.

$$(2.25) \quad \underline{\underline{\Sigma}} = \frac{\partial \Psi}{\partial \underline{\underline{E}}} = \lambda(\text{tr} \underline{\underline{E}}) \underline{\underline{I}} + 2\mu \underline{\underline{E}}$$

$$(2.26) \quad \underline{\underline{\sigma}} = \frac{1}{J} \underline{\underline{F}} \underline{\underline{\Sigma}} \underline{\underline{F}}^T = \begin{bmatrix} \sigma_{xx} & 0 & 0 \\ & \sigma_{yy} & 0 \\ Sym & & \sigma_{zz} \end{bmatrix}$$

The stress components are:

$$(2.27) \quad \sigma_{xx} = \frac{\lambda_1[(\lambda + 2\mu)\lambda_1^2 + \lambda(\lambda_2^2 + \lambda_3^2) - 3 - 2\mu]}{2\lambda_2\lambda_3}$$

$$(2.28) \quad \sigma_{yy} = \frac{\lambda_2[(\lambda + 2\mu)\lambda_2^2 + \lambda(\lambda_1^2 + \lambda_3^2) - 3 - 2\mu]}{2\lambda_1\lambda_3}$$

$$(2.29) \quad \sigma_{zz} = \frac{\lambda_3[(\lambda + 2\mu)\lambda_3^2 + \lambda(\lambda_1^2 + \lambda_2^2) - 3 - 2\mu]}{2\lambda_1\lambda_2}$$

And also the compressibility index:

$$(2.30) \quad J = \lambda_1\lambda_2\lambda_3$$

For such a model we do a test by pulling it in the x - direction. So, the boundary conditions can be defined as below:

$$(2.31) \quad \underline{\underline{\sigma}} \cdot (\pm \underline{\underline{e}}_x) = F \underline{\underline{e}}_x$$

$$(2.32) \quad \underline{\underline{\sigma}} \cdot (\pm \underline{\underline{e}}_y) = 0$$

$$(2.33) \quad \underline{\underline{\sigma}} \cdot (\pm \underline{\underline{e}}_z) = 0$$

The test done on this model is pulling the cube in the x-direction. This test has been done by applying tension from -0.2 MPa to 0.4 MPa. The results are shown in the Figure 2.3.

To solve the inverse problem for different applied force values, a numerical solver is needed to solve the equation and numerically obtain the inverse values. So, we implemented a Newton solver, and in the end, we compared it with the Newton solver of the Python library.

In Figure 2.4 Saint Venant-Kirchhoff model shows logical responses for equitriaxial loading, which means that the more compression, the stiffer the material.

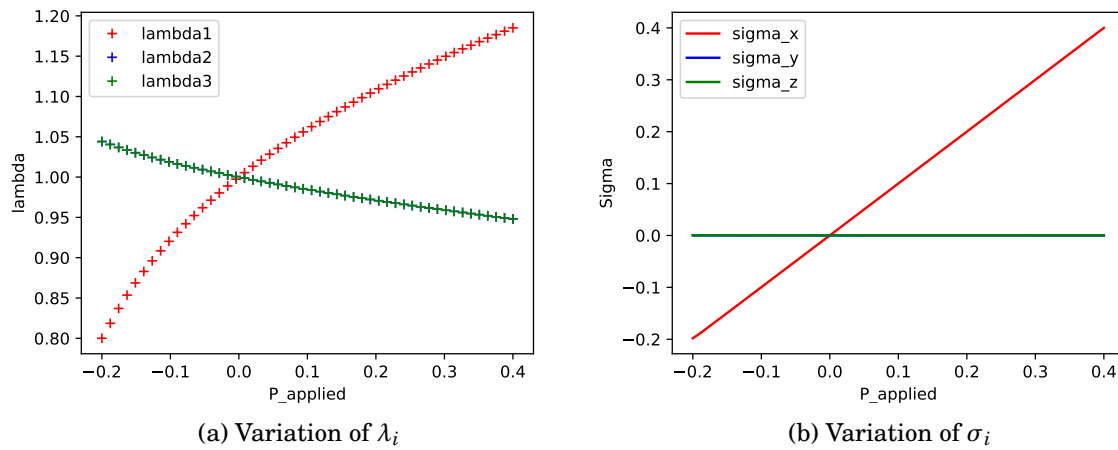


Figure 2.3: The variation of Rivlin cube configuration and stress for the Saint Venant-Kirchhoff model under the applied axial compression in the x- direction

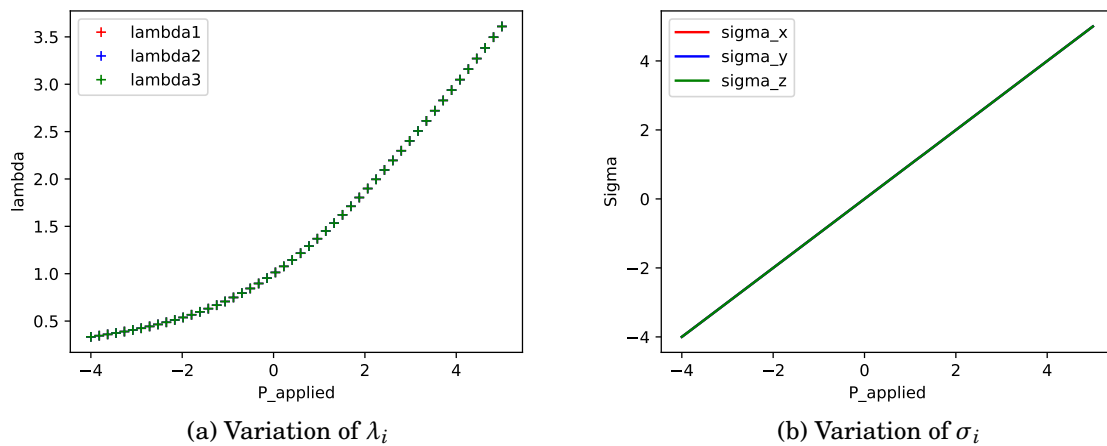


Figure 2.4: The variation of the Rivlin configuration and stress with respect to the equitriaxial pressure applied on the compressible Saint Venant-Kirchhoff model

2.2.3.2 Mooney-Rivlin Model

Mooney-Rivlin energy model is proposed as Equation (2.34)

$$(2.34) \quad \Psi = c_1(\bar{I}_C - 3) + c_2(\bar{II}_C - 3) + \kappa(J^2 - 1 - 2\ln J)$$

Which quantities are defined as below:

$$(2.35) \quad \bar{I}_C = J^{-\frac{2}{3}} I_C$$

$$(2.36) \quad \bar{II}_C = J^{-\frac{4}{3}} II_C$$

$$(2.37) \quad \underline{\underline{C}} = J^{-\frac{2}{3}} \underline{\underline{C}}$$

$$(2.38) \quad \underline{\underline{F}} = J^{\frac{1}{3}} \underline{\underline{F}}$$

For obtaining $\underline{\underline{\Sigma}}$ the following equation can be used:

$$(2.39) \quad \underline{\underline{\Sigma}} = \frac{\partial \Psi}{\partial \underline{\underline{E}}} = 2 \frac{\partial \Psi}{\partial \underline{\underline{C}}} = 2 \frac{\partial \Psi}{\partial \bar{I}_C} \frac{\partial \bar{I}_C}{\partial \underline{\underline{C}}} + 2 \frac{\partial \Psi}{\partial \bar{II}_C} \frac{\partial \bar{II}_C}{\partial \underline{\underline{C}}} + 2 \frac{\partial \Psi}{\partial J} \frac{\partial J}{\partial \underline{\underline{C}}}$$

By the chain rule:

$$(2.40) \quad \frac{\partial \bar{I}_C}{\partial \underline{\underline{C}}} = \frac{\partial \bar{I}_C}{\partial J} \frac{\partial J}{\partial \underline{\underline{C}}}$$

$$(2.41) \quad \frac{\partial J}{\partial \underline{\underline{C}}} = \frac{J}{2} \underline{\underline{C}}^{-1}$$

As a result:

$$(2.42) \quad \frac{\partial \bar{I}_C}{\partial \underline{\underline{C}}} = J^{-\frac{2}{3}} \left(I - \frac{I_C}{3} \underline{\underline{C}}^{-1} \right)$$

$$(2.43) \quad \frac{\partial \bar{II}_C}{\partial \underline{\underline{C}}} = J^{-\frac{4}{3}} \left(I_C I - \underline{\underline{C}} - \frac{2}{3} II_C \underline{\underline{C}}^{-1} \right)$$

For compressible material:

$$(2.44) \quad \underline{\underline{\Sigma}} = 2C_1 J^{-\frac{2}{3}} \left(\underline{\underline{I}} - \frac{I_C}{3} \underline{\underline{C}}^{-1} \right) + 2C_2 J^{-\frac{4}{3}} \left(I_C \underline{\underline{I}} - \underline{\underline{C}} - \frac{2}{3} II_C \underline{\underline{C}}^{-1} \right) + 2\kappa(J^2 - 1) \underline{\underline{C}}^{-1}$$

$$(2.45) \quad \underline{\underline{\sigma}} = \frac{1}{J} \underline{\underline{F}} \underline{\underline{S}} \underline{\underline{F}}^T$$

So:

$$(2.46) \quad \underline{\underline{\sigma}} = 2C_1 J^{-\frac{5}{3}} \left(\underline{\underline{b}} - \frac{I_C}{3} \underline{\underline{I}} \right) + 2C_2 J^{-\frac{7}{3}} \left(I_C \underline{\underline{b}} - \underline{\underline{b}}^2 - \frac{2}{3} I I_C \underline{\underline{I}} \right) + 2\kappa \left(J - \frac{1}{J} \right) C^{-1}$$

It can be supposed $c_1 = c_2 = c_K$. So, $\underline{\underline{\sigma}}$ will be:

$$(2.47) \quad \underline{\underline{\sigma}} = 2c_K \left[J^{-\frac{5}{3}} \left(\underline{\underline{b}} - \frac{I_C}{3} \underline{\underline{I}} \right) + J^{-\frac{7}{3}} \left(I_C \underline{\underline{b}} - \underline{\underline{b}}^2 - \frac{2}{3} I I_C \underline{\underline{I}} \right) \right] + 2\kappa \left(J - \frac{1}{J} \right) C^{-1}$$

For the incompressible model ($J = 1$) and the following relations are true:

$$(2.48) \quad \sigma_{xx} = 2c_K \left[\lambda_1^2 - \frac{\lambda_1^2 + \lambda_2^2 + \lambda_3^2}{3} + (\lambda_1^2 + \lambda_2^2 + \lambda_3^2) \lambda_1^2 - \lambda_1^4 - \frac{2}{3} (\lambda_1^4 + \lambda_2^4 + \lambda_3^4) \right] - \gamma$$

$$(2.49) \quad \sigma_{yy} = 2c_K \left[\lambda_2^2 - \frac{\lambda_1^2 + \lambda_2^2 + \lambda_3^2}{3} + (\lambda_1^2 + \lambda_2^2 + \lambda_3^2) \lambda_2^2 - \lambda_2^4 - \frac{2}{3} (\lambda_1^4 + \lambda_2^4 + \lambda_3^4) \right] - \gamma$$

$$(2.50) \quad \sigma_{zz} = 2c_K \left[\lambda_3^2 - \frac{\lambda_1^2 + \lambda_2^2 + \lambda_3^2}{3} + (\lambda_1^2 + \lambda_2^2 + \lambda_3^2) \lambda_3^2 - \lambda_3^4 - \frac{2}{3} (\lambda_1^4 + \lambda_2^4 + \lambda_3^4) \right] - \gamma$$

In which γ is the hydro-static pressure. For the incompressible model another relation exists:

$$(2.51) \quad J = \lambda_1 \lambda_2 \lambda_3 = 1$$

By applying the boundary conditions as below:

$$(2.52) \quad \underline{\underline{\sigma}} \cdot (\pm \underline{\underline{e}}_x) = F \underline{\underline{e}}_x$$

$$(2.53) \quad \underline{\underline{\sigma}} \cdot (\pm \underline{\underline{e}}_y) = 0$$

$$(2.54) \quad \underline{\underline{\sigma}} \cdot (\pm \underline{\underline{e}}_z) = 0$$

The following relation comes true:

$$(2.55) \quad \lambda_3 = \lambda_2$$

So:

$$(2.56) \quad \lambda_3^2 = \lambda_2^2 = \frac{1}{\lambda_1}$$

There are two equations with the applied pressure P :

$$(2.57) \quad \lambda_1^2 - \frac{\lambda_1^2}{3} - \frac{2}{3\lambda_1} + \left(\lambda_1^2 + \frac{2}{\lambda} \right) \lambda_1^2 - \lambda_1^4 - \frac{2}{3} \left(\lambda_1^4 + \frac{2}{\lambda^2} \right) - \gamma = P$$

$$(2.58) \quad \frac{1}{\lambda_1} - \frac{\lambda_1^2}{3} - \frac{2}{3\lambda_1} + \left(\lambda_1^2 + \frac{2}{\lambda}\right) \frac{1}{\lambda_1} - \frac{1}{\lambda_1^2} - \frac{2}{3} \left(\lambda_1^4 + \frac{2}{\lambda^2}\right) - \gamma = 0$$

By subtracting the second equation from the first one, γ can be omitted.

$$(2.59) \quad \lambda_1^2 + \lambda_1 - \frac{1}{\lambda_1} - \frac{1}{\lambda_1^2} = P$$

For linearization, following relation can be implemented:

$$(2.60) \quad \underline{J} \approx 1 + tr(\underline{\epsilon})$$

$$(2.61) \quad \underline{b} \approx 1 + 2\underline{\epsilon}$$

$$(2.62) \quad \underline{b}^2 \approx 1 + 4\underline{\epsilon}$$

$$(2.63) \quad \underline{C} \approx 1 + 2\underline{\epsilon}$$

$$(2.64) \quad I_C \approx 3 + 2tr(\underline{\epsilon})$$

$$(2.65) \quad II_C \approx 3 + 4tr(\underline{\epsilon})$$

So, the linearized stress-strain relation can be written as below:

$$(2.66) \quad \underline{\underline{\sigma}} \approx 4(c_1 + c_2 + \kappa)\underline{\underline{\epsilon}} + 4\left(\kappa - \frac{(c_1 + c_2)}{3}\right)tr(\underline{\underline{\epsilon}})\underline{\underline{I}}$$

$$(2.67) \quad \underline{\underline{\epsilon}} = \underline{\underline{F}} - \underline{\underline{I}}$$

By supposing that

$$(2.68) \quad \kappa = \lambda/2$$

When there is no stress on the cube, it doesn't have any deformation, it mean:

$$(2.69) \quad \lambda_1 = \lambda_2 = \lambda_3 = 1$$

And for such a special condition

$$(2.70) \quad \underline{\underline{\sigma}} \cdot (\pm \underline{e}_x) = 0$$

$$(2.71) \quad \underline{\underline{\sigma}} \cdot (\pm \underline{e}_y) = 0$$

$$(2.72) \quad \underline{\underline{\sigma}} \cdot (\pm \underline{e}_z) = 0$$

By applying force in the x-direction on the compressible Mooney-Rivlin model, the result obtained in Figure 2.5. By applying force in the equitriaxial direction on the compressible Mooney-Rivlin model, the result shown in Figure 2.6.

The same test had been done on the incompressible Mooney-Rivlin model. One test applied the pressure in the x-direction, which results are shown in the Figure 2.7. The other test is applying equitriaxial pressure as in Figure 2.8. As expected, the notable point is that there is no dimension change for the incompressible models in compression and tension. Moreover, the same result is for the Saint Venant-Kirchhoff model.

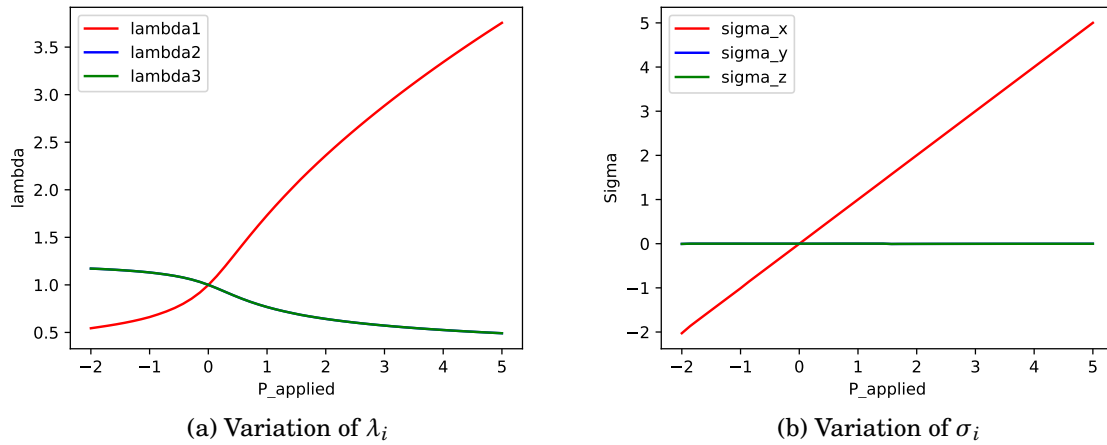


Figure 2.5: The variation of Rivlin cube configuration and stress with respect to applied axial pressure for the compressible Mooney-Rivlin model

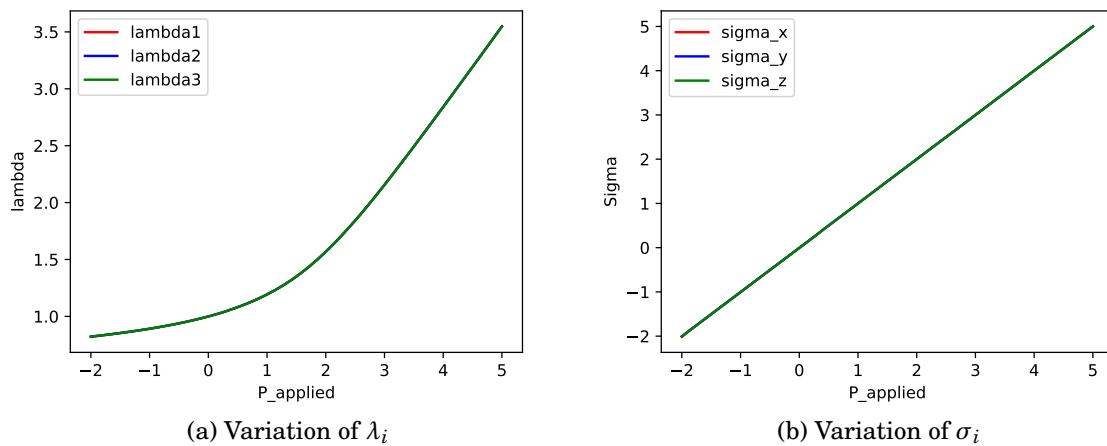


Figure 2.6: The variation of Rivlin cube configuration and stress with respect to applied equibiaxial pressure for the compressible Mooney-Rivlin model

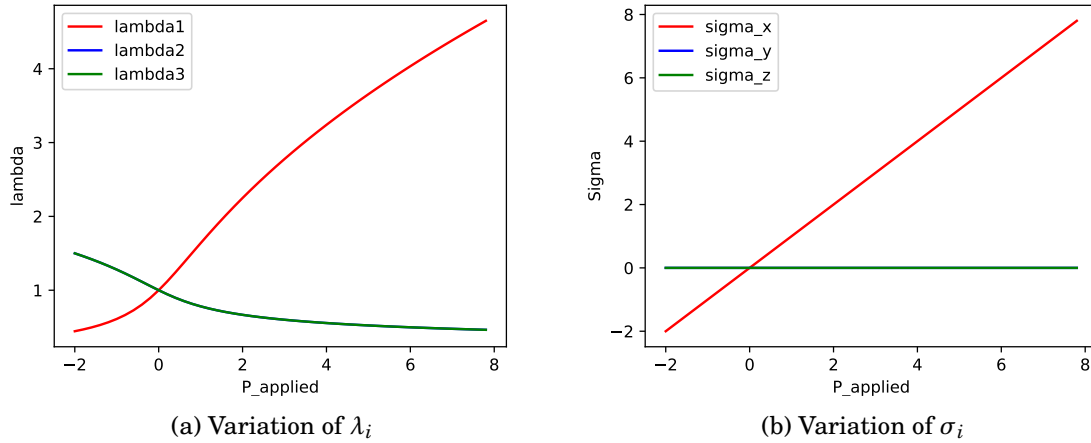


Figure 2.7: The variation of Rivlin cube configuration and stress with respect to applied axial pressure for the incompressible Mooney-Rivlin model

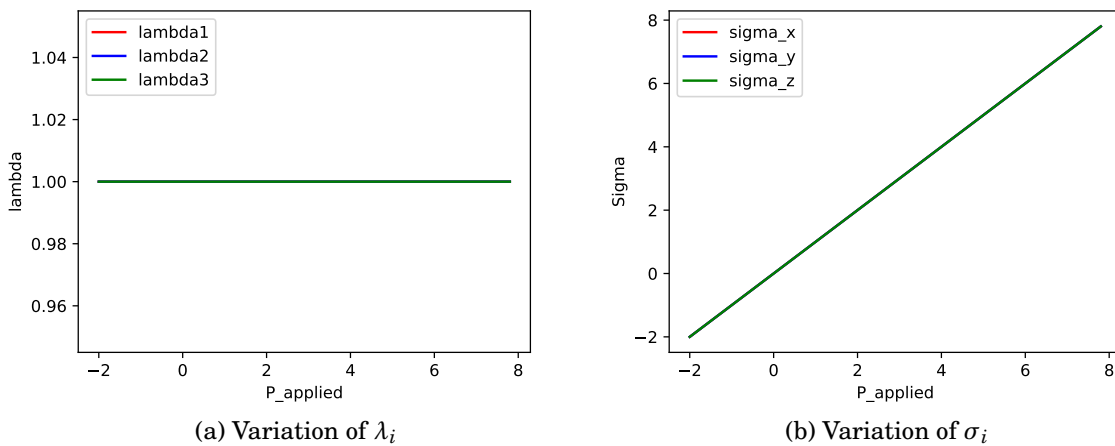


Figure 2.8: The variation of Rivlin cube configuration and stress with respect to applied equibiaxial pressure for the incompressible Mooney-Rivlin model

2.2.3.3 Analysis of the Bulk Energy Forms

A form of energy for the Mooney-Rivlin model has been chosen, but the bulk energy can have different forms. Here these different forms of energy have been discussed in the following:

$$(2.73) \quad \Psi_1 = J - 1 - \ln J$$

$$(2.74) \quad \Psi_2 = (J - 1 - \ln J)^2$$

$$(2.75) \quad \Psi_3 = J^2 - 1 - 2\ln J$$

These three different forms of the bulk energy can be shown qualitatively in Figure 2.9. All

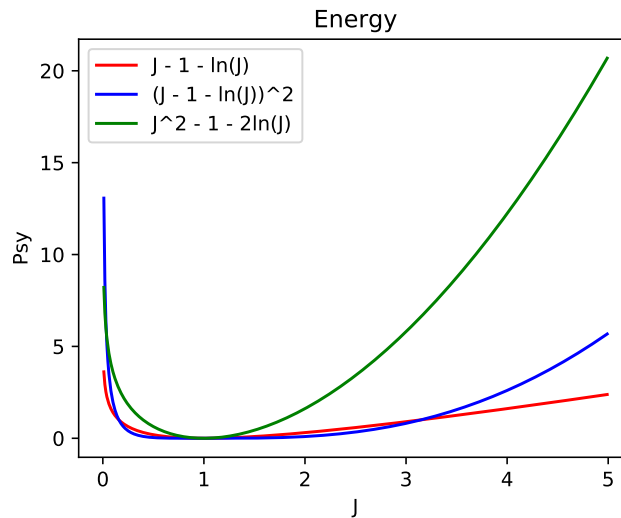


Figure 2.9: Three different bulk energy models variation with respect to the compression index

energy form are suitable up to now, as they are all infinity in zero and minimum equal zero when we have no deformation ($J = 1$) and infinity when J goes to infinity. The first derivative of the bulk energy forms are as the following:

$$(2.76) \quad \frac{\partial \Psi_1}{\partial J} = 1 - \frac{1}{J}$$

$$(2.77) \quad \frac{\partial \Psi_2}{\partial J} = 2(J - 1 - \ln J) \left(1 - \frac{1}{J}\right)$$

$$(2.78) \quad \frac{\partial \Psi_3}{\partial J} = 2\left(J - \frac{1}{J}\right)$$

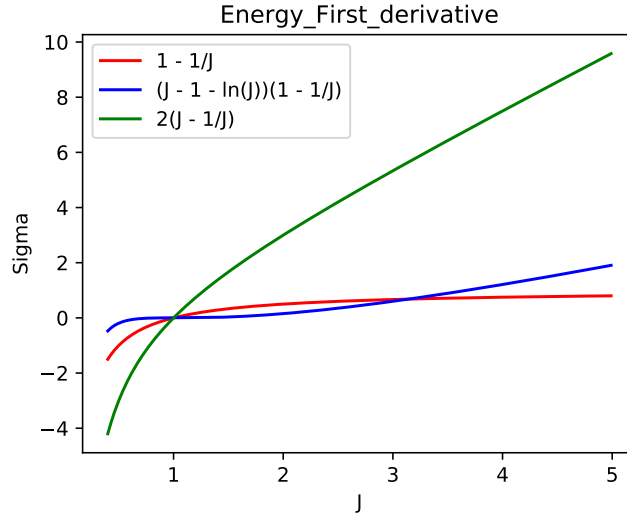


Figure 2.10: First derivative of three different bulk energy models variation with respect to the compression index

First derivative of these three different forms of the bulk energy can be shown qualitatively in (Figure 2.10.)

The first derivative of energy is related to stress. It is evident that for the first energy model, the stress is limited in infinity. It means that there is no solution for stress applied more than the limited value; in other words, “J” is equal to infinity for such stress.

$$(2.79) \quad \frac{\partial^2 \Psi_1}{\partial J^2} = \frac{1}{J^2}$$

$$(2.80) \quad \frac{\partial^2 \Psi_2}{\partial J^2} = 2 \left(1 - \frac{1}{J} - \frac{\ln J}{J^2} \right)$$

$$(2.81) \quad \frac{\partial^2 \Psi_3}{\partial J^2} = 2 \left(1 + \frac{1}{J^2} \right)$$

Second derivative of these three different forms of the bulk energy can be shown qualitatively in (Figure 2.11.)

The second energy, which shows the stiffness coefficient, is zero at rest position, which is not proper, and also the first one has the stiffness equal to zero in the infinity, which is not meaningful either.

2.2.3.4 Nonlinearity of the Rivlin Cube

After pulling the Rivlin cube with specific pressure, the minus pressure can be applied to the deformed cube to illustrate the model non-linearity. For example, if the extension with value

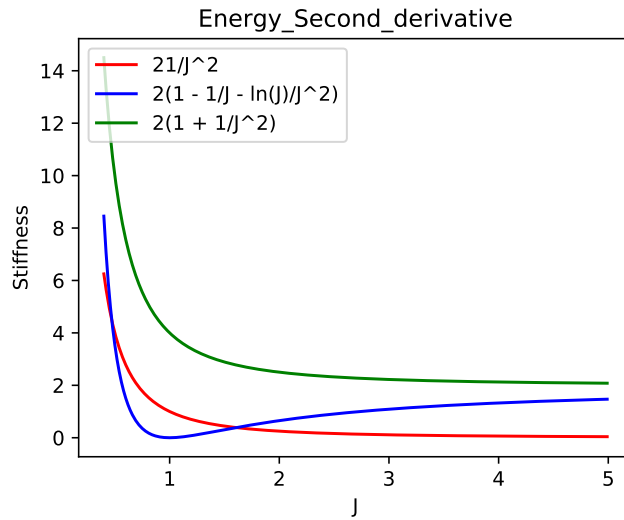


Figure 2.11: Second derivative of three different bulk energy models variation with respect to the compression index

of $P = 0.2 \text{ MPa}$ can be applied in the x-direction to a cube with dimension 10, it leads to the following configuration:

$$(2.82) \quad \underline{X1} = \begin{bmatrix} 11.9575926911927 \\ 9.58610080999857 \\ 9.58610080999857 \end{bmatrix}$$

And by applying the minus value of the last applied pressure $P = -0.2 \text{ MPa}$ on the above configuration, it leads to the following configuration:

$$(2.83) \quad \underline{X2} = \begin{bmatrix} 10.6963257156302 \\ 9.93319594415821 \\ 9.93319594415821 \end{bmatrix}$$

Which is not the same configuration we started with.

2.3 Inverse Problem

This kind of problem is the most important one is very applicable in biomechanics as there are many problems that the unloaded configuration or material parameter is not known, or it can be the combination of these two. What are known in these kinds of problems are the applied force and some measured deformed configuration. So, it is needed as many data points as the unknown parameters. These parameters can be material parameters or the undeformed configuration, which depends on the coordinates. In the following, all cases of the mentioned materials will be discussed.

The golden point which will be presented in the following is that besides the material parameter estimation, only one additional data point is needed for estimation of the unloaded configuration.

2.3.1 Methods for Minimizing a Cost Function

2.3.1.1 Gradient Free Method (CMA)

This method is the least efficient method for finding a minimum for the cost function. It does check different parameters in a specific domain and find the least value of the cost function corresponding to the guessed parameters values. CMA² algorithm has been used for minimizing the cost function by this method.

2.3.1.2 Newton Solver

For the hyperelastic model the stress tensor $\underline{\underline{\sigma}}(\underline{\lambda})$ should be equal to the applied pressure \underline{P} , but as an initial guess like $\underline{\lambda}_0$ we have a residual which is the difference between the stress tensor and the applied pressure vector:

$$(2.84) \quad \underline{R}_0 = \underline{\underline{\sigma}}(\underline{\lambda}_0) - \underline{P}$$

In the above equation, $\underline{\underline{\sigma}}$ and \underline{P} are defined as below:

$$(2.85) \quad \underline{\underline{\sigma}} = \begin{bmatrix} \sigma_{11} \\ \sigma_{22} \\ \sigma_{33} \end{bmatrix}$$

$$(2.86) \quad \underline{P} = \begin{bmatrix} P_1 \\ P_2 \\ P_3 \end{bmatrix}$$

And:

$$(2.87) \quad \underline{R}_0 = \begin{bmatrix} \sigma_{11} - P_1 \\ \sigma_{22} - P_2 \\ \sigma_{33} - P_3 \end{bmatrix}$$

By writing Taylor expansion around λ_0 , the updated law can be obtained.

$$(2.88) \quad \underline{\underline{\sigma}}(\underline{\lambda}_0 + \underline{\Delta\lambda}) \approx \underline{\underline{\sigma}}(\underline{\lambda}_0) + \frac{\partial \underline{\underline{\sigma}}}{\partial \underline{\lambda}}(\underline{\lambda}_0) \cdot \underline{\Delta\lambda}$$

As the following equation exists:

$$(2.89) \quad \underline{\underline{\sigma}}(\underline{\lambda}_0 + \underline{\Delta\lambda}) = \underline{P}$$

²Covariance Matrix Adaptation Evolution Strategy

So, the update law would be like Equation (2.90)

$$(2.90) \quad \underline{\Delta\lambda_0} = \frac{\underline{P} - \underline{\sigma}(\underline{\lambda_0})}{\frac{\partial \underline{\sigma}}{\partial \underline{\lambda}}(\underline{\lambda_0})} = -\underline{Jac}^{-1} \cdot \underline{R_0}$$

In which Jac is Jacobian matrix of σ :

$$(2.91) \quad \underline{Jac} = \frac{\partial \underline{\sigma}}{\partial \underline{\lambda}}$$

What has been done here is that the cost function should be minimized, which means that its gradient should become zero. So, the Newton method has been done on the derivative of the cost function.

2.3.1.3 Gradient Descent Method

This method is somehow a more straightforward Newton solver, which converges after some steps to the minimum cost function. It can be described as below:

$$(2.92) \quad x_{n+1} = x_n - \gamma_n \nabla F(x_n)$$

In which γ_n can be described as:

$$(2.93) \quad \gamma_n = \frac{|(x_n - x_{n-1})^T [\nabla F(x_n) - \nabla F(x_{n-1})]|}{\|\nabla F(x_n) - \nabla F(x_{n-1})\|^2}$$

In this paper γ_0 has been considered as 1.

2.3.2 Methods for Computing Gradients and Hessians

So far, different cost functions for the different inverse problems have been suggested, and a common characteristic between them is the convexity of the cost function near the exact value of material parameters or zero with normalized parameters. The existence of a solution for parameters depends on the convexity of the cost function near the solution. So, criteria to chase the behavior of the cost function.

2.3.2.1 Finite difference approximation

The cost function behavior can be predicted by obtaining the gradient or Hessian matrix, and the cost function eigenvalues on the convex point. This can be done numerically and analytically in general. Here it is shown that the gradient of some cost functions numerically can be obtained, with finite difference method.

Two things are calculable here. One is the gradient of the cost function on each point, which is

applicable for solving the Newton method. Most of the time, the cost function is complicated, that the gradient can not be calculated analytically. So, it is needed to calculate it numerically. The numerical gradient of the cost function J with two parameters in a specified point θ can be determined below:

$$(2.94) \quad \underline{Grad}(J(\theta)) = \begin{bmatrix} \frac{J(\frac{h}{2}, 0) - J(-\frac{h}{2}, 0)}{h} \\ \frac{J(0, \frac{h}{2}) - J(0, -\frac{h}{2})}{h} \end{bmatrix}$$

An for a cost function with three parameters (like a nonlinear spring) it would be:

$$(2.95) \quad \underline{Grad}(J(\theta)) = \begin{bmatrix} \frac{J(\frac{h}{2}, 0, 0) - J(-\frac{h}{2}, 0, 0)}{h} \\ \frac{J(0, \frac{h}{2}, 0) - J(0, -\frac{h}{2}, 0)}{h} \\ \frac{J(0, 0, \frac{h}{2}) - J(0, 0, -\frac{h}{2})}{h} \end{bmatrix}$$

One crucial point here is the existence of a minimum for the cost function. The existence of the minimum can be recognized by Hessian matrix. Hessian matrix can be calculated as below:

$$\underline{\underline{H}}(f) = \begin{pmatrix} \frac{\partial^2 f}{\partial x_1^2} & \frac{\partial^2 f}{\partial x_1 \partial x_2} & \cdots & \frac{\partial^2 f}{\partial x_1 \partial x_n} \\ \frac{\partial^2 f}{\partial x_2 \partial x_1} & \frac{\partial^2 f}{\partial x_2^2} & \cdots & \frac{\partial^2 f}{\partial x_2 \partial x_n} \\ \vdots & \vdots & \ddots & \vdots \\ \frac{\partial^2 f}{\partial x_n \partial x_1} & \frac{\partial^2 f}{\partial x_n \partial x_2} & \cdots & \frac{\partial^2 f}{\partial x_n^2} \end{pmatrix}$$

In which the second derivative would be obtained numerically:

$$(2.96) \quad \frac{\partial^2 f}{\partial x_1 \partial x_2} = \frac{f(h, h) - f(0, h) - f(h, 0) + f(0, 0)}{h^2}$$

In which h value supposed a minimal value like 10^{-6} .

2.3.2.2 The Adjoint Method

The most important thing we need, is the derivative of the cost function- which can be defined as below- with respect to the unknown parameter:

$$(2.97) \quad J(\theta) = \int_{\Omega} j(u_{\theta}) + \frac{\beta}{2} \|\theta - \theta_0\|^2$$

In which $j(\theta)$ can be as an instant:

$$(2.98) \quad j(u_{\theta}) = (u - u^{mes})$$

For obtaining the derivative of the cost function with respect to the parameter we would define the "adjoint problem":

$$(2.99) \quad \hat{J}(\theta, u) = \int_{\Omega} j(u) + \frac{\beta}{2} \|\theta - \theta_0\|^2$$

In which u is supposed independant to θ . And here Lagrangian is defined as:

$$(2.100) \quad L(\theta, u, \lambda) = \hat{J}(\theta, u) + W_{int}(u, \lambda) - W_{ext}(\lambda)$$

By doing the finite differentiation with respect to variables:

$$(2.101) \quad \delta_u L \cdot u^* = \delta_u \hat{J} \cdot u^* + W_{int}(u^*, \lambda) = 0$$

$$(2.102) \quad \delta_\lambda L \cdot \lambda^* = W_{int}(u, \lambda^*) - W_{ext}(\lambda^*) = 0$$

There is:

$$(2.103) \quad \delta_u L \cdot u^* = \delta_u J \cdot u^*$$

As a conclusion:

$$(2.104) \quad L(\theta, u, \lambda) = \hat{J}(\theta, u) = J(\theta)$$

$$(2.105) \quad \frac{\partial J}{\partial \theta} \cdot \theta^* = \frac{\partial L}{\partial \theta} \cdot \theta^* + \frac{\partial L}{\partial u} \frac{\partial u}{\partial \theta} \cdot \theta^*$$

As a result:

$$(2.106) \quad \frac{\partial J}{\partial \theta} = \frac{\partial L}{\partial \theta}(\theta, u, \lambda)$$

2.3.2.3 Linear Spring

The cost function for solving the inverse problem of the spring can be written as below as mentioned before:

$$(2.107) \quad J(K) = \frac{1}{2} (u_K - u^{mes})^2$$

For this simple problem, the derivative of the cost function concerning the material parameter can be obtained easily:

$$(2.108) \quad \frac{\partial J}{\partial K} = \frac{\partial J}{\partial u} \frac{\partial u}{\partial K} = -(u_K - u^{mes}) \frac{F}{K^2}$$

As in the linear spring $u = \frac{F}{K} + u_0$. However, by implementing the mentioned method, the adjoint problem can be defined for that:

$$(2.109) \quad \hat{J} = \frac{1}{2} (u - u^{mes})^2$$

So, Lagrangian can be written as:

$$(2.110) \quad L = \frac{1}{2} (u - u^{mes}) + \lambda (K(u - u_0) - F)$$

Like the last part, it can be written as below:

$$(2.111) \quad \delta_u \hat{J} \cdot u^* = -W_{int}(u^*, \lambda)$$

Which means:

$$(2.112) \quad \lambda K u^* + (u - u^{mes}) u^* = 0$$

And from the equation (2.102):

$$(2.113) \quad u = \frac{F}{K} + u_0$$

As a conclusion:

$$(2.114) \quad \lambda = \frac{-(u - u^{mes})}{K}$$

And the derivative of the Lagrangian with respect to the material parameter:

$$(2.115) \quad \frac{\partial L}{\partial K} = \lambda(u - u_0)$$

So from the equations (2.114) and (2.115) the gradient of the cost function with respect to the material parameter can be obtained:

$$(2.116) \quad \frac{\partial J}{\partial K} = \frac{-(u - u^{mes})F}{K^2}$$

2.3.2.4 Linear Elasticity

The same problem for the linear elasticity problem in continuum mechanics can be solved. In the linear elasticity the Hooke's law is as below:

$$(2.117) \quad \underline{\underline{\sigma}} = 2\mu \underline{\underline{\epsilon}} + \lambda \text{tr}(\underline{\underline{\epsilon}}) \underline{\underline{I}}$$

Here the virtual work of the internal and external forces can be defined as below:

$$(2.118) \quad W_{int}(u, u^*) = \int_{\Omega} \underline{\underline{\epsilon}}(u) : \underline{\underline{C}} : \underline{\underline{\epsilon}}(u^*)$$

$$(2.119) \quad W_{ext}(u^*) = \int_{\partial\Omega} \underline{\underline{F}} \cdot \underline{\underline{u}}^* + \int_{\Omega} \underline{\underline{f}} \cdot \underline{\underline{u}}^*$$

By assuming $W_{int} = W_{ext}$ can obtain the strong form of the equations:

$$(2.120) \quad \text{div} \underline{\underline{\sigma}} + \underline{\underline{f}} = 0, \text{ in } \Omega$$

$$(2.121) \quad \underline{\underline{\sigma}} \cdot \underline{\underline{n}} = \underline{\underline{F}}, \text{ on } \partial\Omega$$

2.3.3 Unloaded Configuration Estimation

2.3.3.1 Linear Spring

Suppose the known parameters are the deformed length of the spring, applied force, and the stiffness coefficient, but the spring undeformed length is unknown. There is one unknown here, and the undeformed length of the spring can be estimated as the following equation:

$$(2.135) \quad \underline{u}^{\text{undef}} = u^{\text{def}} - \frac{F}{E}$$

2.3.3.2 Rivlin Cube

The inverse problem for the Rivlin cube for obtaining the unloaded configuration is such that the applied force and a loaded configuration are known, and the unloaded configuration is the goal. The applied force can be supposed as below:

$$(2.136) \quad \underline{\underline{F}} = \begin{bmatrix} F_1 & 0 & 0 \\ 0 & F_2 & 0 \\ 0 & 0 & F_3 \end{bmatrix}$$

And the deformed configuration is supposed is below:

$$(2.137) \quad \underline{\underline{X1}} = \begin{bmatrix} X \\ Y \\ Z \end{bmatrix}$$

While $X = \lambda_1 x$, $Y = \lambda_2 y$ and $Z = \lambda_3 z$. So, for finding the undeformed configuration x , y and z , three equations needed to be solved for finding the unloaded configuration:

$$(2.138) \quad F_1 = \lambda_1 x$$

$$(2.139) \quad F_2 = \lambda_2 y$$

$$(2.140) \quad F_3 = \lambda_3 z$$

Saint Venant-Kirchoff is not a good model. To show this fact, the displacement control test was done, and the results, as shown in (Figure 2.12) is that when applying the displacement change in the x-direction, the pressure in the x direction is limited. This means that we cannot have any solution for the displacement when we apply a pressure beyond that limit. This shows that the Saint Venant-Kirchhoff model is not good as when the cube is compressed, it will become less stiff, and it would be easier to compress the cube. The other test is applying pressure on the Saint Venant-Kirchhoff Cube in the equitriaxial direction. It means that there is the same pressure in all directions. Another test can be done on this cube, which is controlling the displacement. The λ_i is changing during this test, and the variation of the pressure is visible in (Figure 2.12)

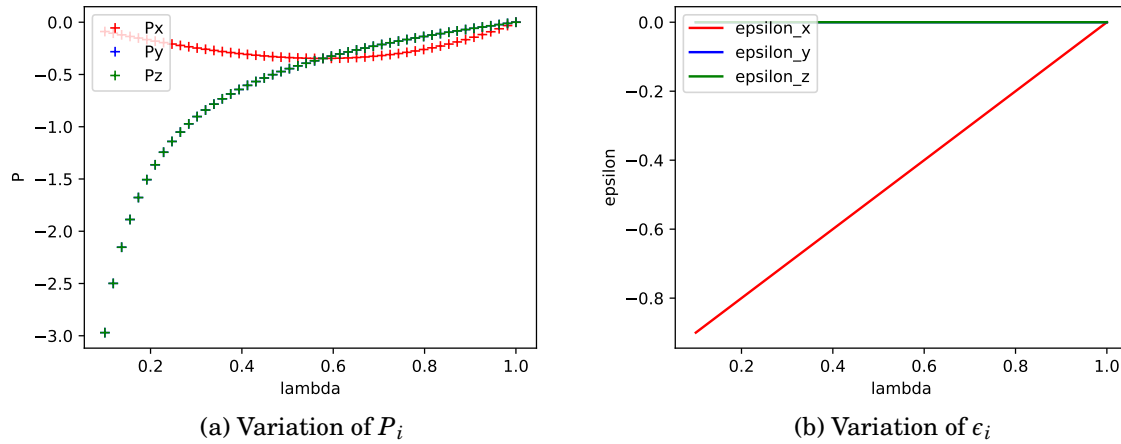


Figure 2.12: The variation of the pressure and displacement with respect to the lambda for the compressible Saint Venant-Kirchhoff model

2.3.4 Material Parameter Estimation

2.3.4.1 Linear Spring

There is another kind of problem in which the deformed and undeformed configuration is known while the material property, like the stiffness coefficient here, is unknown, which can be obtained by the Equation (2.141).

$$(2.141) \quad E = \frac{F}{u^{def} - u^{undef}}$$

This simple problem can be solved by minimizing the cost function as defined in the Equation (2.142).

$$(2.142) \quad J(E) = \frac{1}{2} \frac{(u^{def} - u^{mes})^2}{(u^{mes2})^2}$$

u^{mes} is what is known from the measurement and:

$$(2.143) \quad u^{def} = \frac{F}{E} + u^{undef}$$

In Equation (2.143), F and u^{undef} are known. The minimization of this function is done by assuming $u^{undef} = 0.1 \text{ mm}$, $u^{def} = 0.2 \text{ mm}$ and applied force $F = 1 \text{ N}$. This minimization can be done by hand quickly, but CMA is used here to validate the data. The result of the minimization by CMA is shown in Figure 2.13.

Figure 2.13 shows the minimization of the cost function for the linear spring for finding the stiffness coefficient. CMA code has done lots of attempts for the given domain to find a minimum for the cost function.

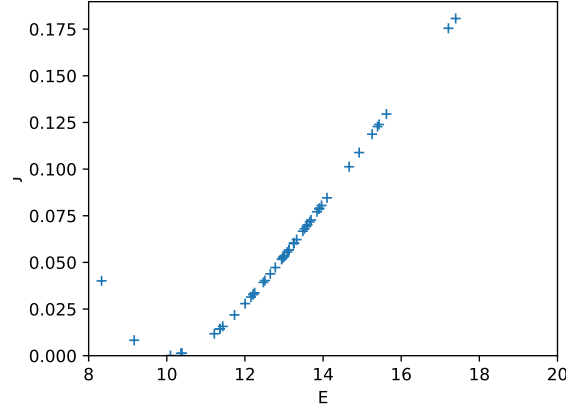


Figure 2.13: Minimizing the cost function ($J(E)$) by CMA code for the linear spring.

2.3.4.2 Rivlin Cube

As mentioned in section 2.2.3.1, in the Saint Venant-Kirchhoff model, there are two material parameters λ and μ . In solving the inverse problem for the material parameters, it is needed two equations.

An analytical solution is presented when an equitriaxial pressure is applied on the cube with the Saint Venant-Kirchhoff model. In this specific condition: $\lambda_1 = \lambda_2 = \lambda_3 = \lambda_0$. So, the relation between λ and the applied pressure, can be obtained as below:

$$(2.144) \quad \lambda = \frac{P + \sqrt{P^2 + (3\lambda_0 + \mu)(3 + 2\mu)}}{(3\lambda_0 + \mu)}$$

By applying different pressures, the variation of λ with respect to the applied pressure can be plotted as Figure 2.14. For incompressible materials:

$$(2.145) \quad \underline{\underline{\Sigma}} = \frac{\partial \Psi}{\partial \underline{\underline{E}}} = \lambda(\text{tr} \underline{\underline{E}}) + 2\mu \underline{\underline{E}} - \gamma J \underline{\underline{C}}^{-1}$$

for the incompressible materials, $J = 1$, so:

$$(2.146) \quad \lambda_3 = \frac{1}{\lambda_1 \lambda_2}$$

$$(2.147) \quad \sigma_{xx} = \frac{\lambda_1^2 [(\lambda + 2\mu)\lambda_1^2 + \lambda(\lambda_2^2 + \frac{1}{\lambda_1^2 \lambda_1^2}) - 3 - 2\mu]}{2} - \frac{\gamma}{\lambda_1^2}$$

$$(2.148) \quad \sigma_{yy} = \frac{\lambda_2^2 [(\lambda + 2\mu)\lambda_2^2 + \lambda(\lambda_1^2 + \frac{1}{\lambda_1^2 \lambda_2^2}) - 3 - 2\mu]}{2} - \frac{\gamma}{\lambda_2^2}$$

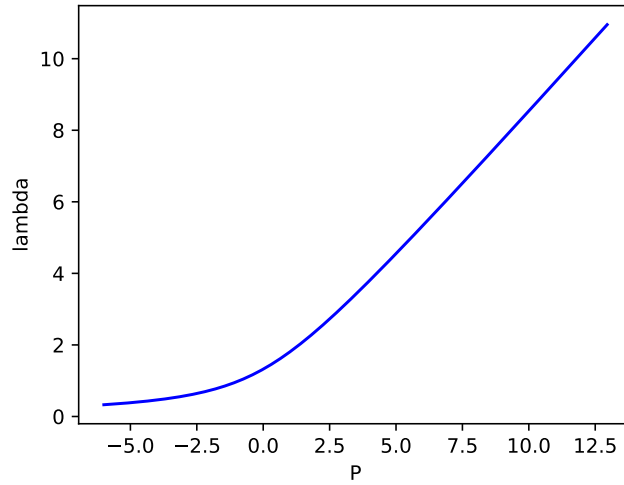


Figure 2.14: The variation of λ in Saint-Venant Kirchhoff model with respect to the applied equitriaxial pressure applied on Rivlin Cube

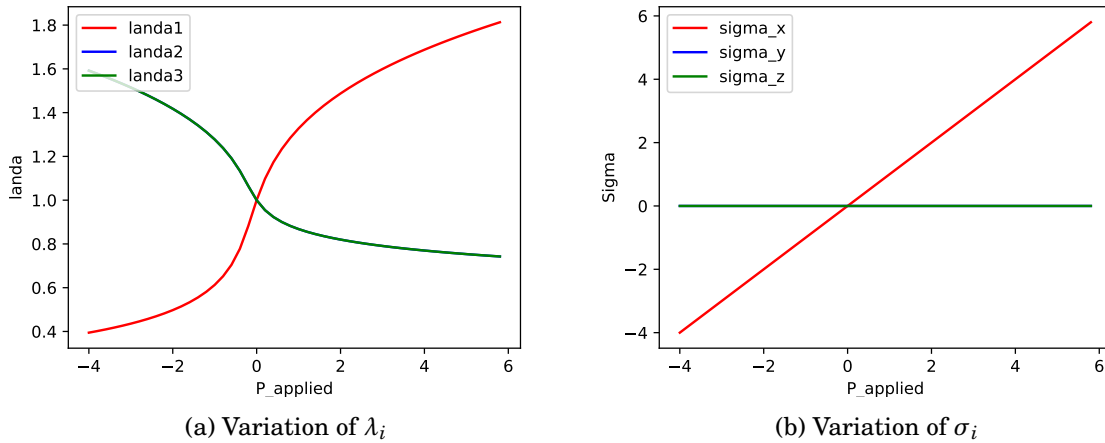


Figure 2.15: The variation of Rivlin cube configuration and stress with respect to applied axial pressure for the incompressible Saint-Venant Kirchhoff model

$$(2.149) \quad \sigma_{zz} = \frac{[(\lambda + 2\mu) \frac{1}{\lambda_1^2 \lambda_2^2} + \lambda(\lambda_1^2 + \lambda_2^2) - 3 - 2\mu]}{2\lambda_1^2 \lambda_2^2} - \gamma \lambda_1^2 \lambda_2^2$$

The previous tests on the compressible material are also done on the incompressible material. The results for the applied force in the x-direction is Figure 2.15. For the equitriaxial applied force, the results are as Figure 2.16.

There are two unknowns as the parameters of this model, like μ and λ . So, two data points

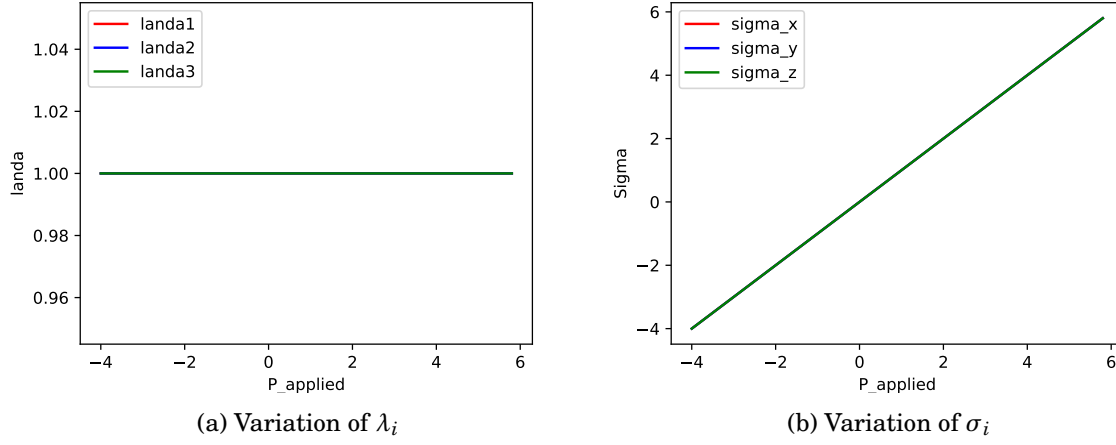


Figure 2.16: The variation of Rivlin cube configuration and stress with respect to applied equitri-axial pressure for the incompressible Saint-Venant Kirchhoff model

are needed to minimize this cost function.

$$(2.150) \quad J = \frac{1}{2} \left\{ \frac{[X_1 - X_1^{mes}]^2}{[X_1^{mes}]^2} + \frac{[X_2 - X_2^{mes}]^2}{[X_2^{mes}]^2} \right\}$$

In which X_i^{mes} is the measured configuration, and X_i is the calculated configuration. The problem here is obtaining the calculated configuration. Supposing the relation below, which was discussed before:

$$(2.151) \quad \underline{\underline{\sigma}} = (2\mu(\underline{\underline{b}} - \underline{\underline{I}}) + 2\lambda(I_C \underline{\underline{b}} - \underline{\underline{b}}^2 - 2\underline{\underline{I}}))/J + 2\kappa(J - 1/J)\underline{\underline{C}}^{-1}$$

As here the matrix $\underline{\underline{C}}$ contains λ_1 , λ_2 and λ_3 , beside the forces applied on the cube, there are three equations to solve:

$$(2.152) \quad \sigma_x = P_x$$

$$(2.153) \quad \sigma_y = P_y$$

$$(2.154) \quad \sigma_z = P_z$$

From the above equations, λ_1 , λ_2 and λ_3 would be obtained with respect to μ and λ . So, now the cost function is only a function of μ and λ , which should be minimized. In section 1.5, it is explained how to minimize the cost function. For the Mooney-Rivlin model, the cost function concerning the dimensionless variables is shown in Figure 2.17, and the minimization of each parameter is shown in Figure 2.18.

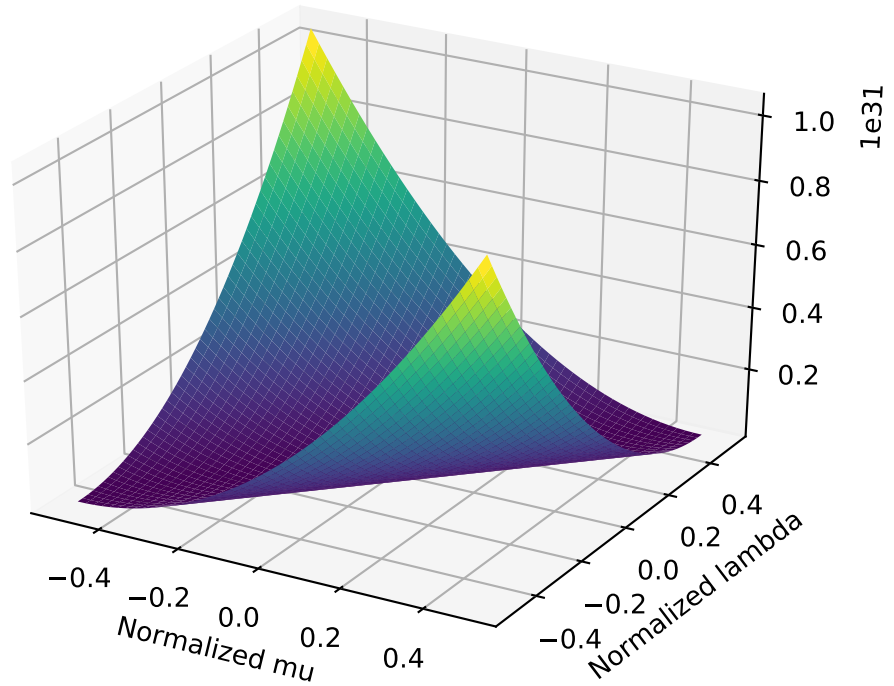


Figure 2.17: Minimization of Mooney-Rivlin cube cost function with respect to re-scaled material parameters λ and μ .

2.3.5 Combined Estimation of the Unloaded Configuration and Material Parameters

2.3.5.1 Linear Spring

The more important problem is when the undeformed length or the stiffness of the spring is not known. This problem importance is that because it is a classic problem in biomechanics where the unloaded configuration and the material parameters are unknown most of the time. In this problem, the known data are the deformed configuration and the applied force, but as there are two unknowns: the undeformed configuration and the stiffness coefficient, two sets of data points are needed.

$$(2.155) \quad E(u_1^{mes} - u_{undef}) = F_1^{mes}$$

$$(2.156) \quad E(u_2^{mes} - u_{undef}) = F_2^{mes}$$

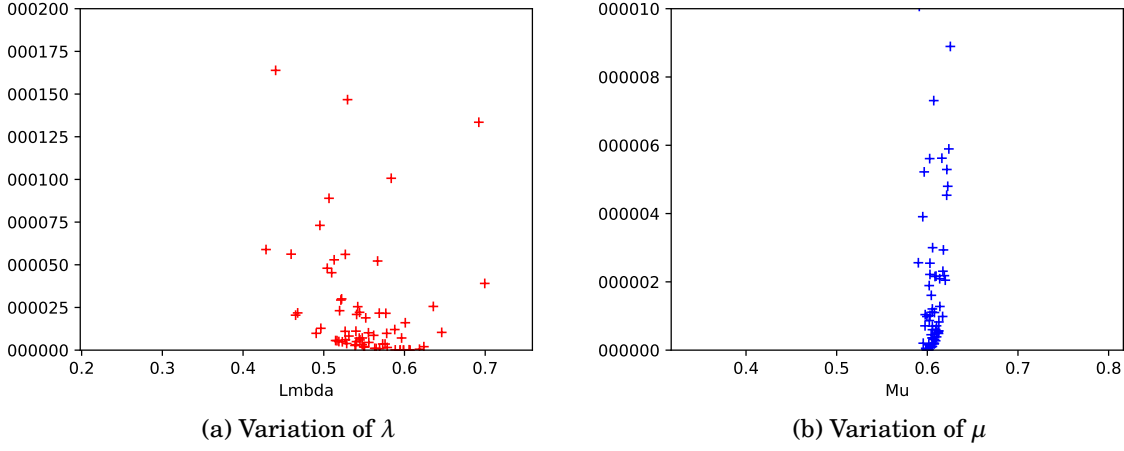


Figure 2.18: Minimization of Mooney-Rivlin cube cost function with respect to re-scaled material parameters λ and μ .

From the above equations E and u_{undef} can be obtained.

$$(2.157) \quad E = \frac{F_2^{mes} - F_1^{mes}}{u_2^{mes} - u_1^{mes}}$$

And

$$(2.158) \quad u_{undef} = u_1^{mes} - \frac{F_1^{mes}}{F_2^{mes} - F_1^{mes}}(u_2^{mes} - u_1^{mes})$$

Now a problem can be defined and solved with two different approaches. Supposing $u_1 = 0.2 \text{ mm}$ and $F_1 = 1 \text{ N}$ and another data point as $u_2 = 0.22 \text{ mm}$ and $F_2 = 1.2 \text{ N}$, here there are two equations and two unknowns. With the above equations:

$$(2.159) \quad E = 10$$

$$(2.160) \quad u_{undef} = 0.1$$

Of course, this problem is easy enough to be solved by hand, but CMA optimizer can be used for validation such that it minimizes J concerning E and u_{undef} , which is defined as Equation (2.161).

$$(2.161) \quad J(E, u_{undef}) = \frac{1}{2} \left(\frac{(U_1 - u_1^{mes})^2}{u_1^{mes2}} + \frac{(U_2 - u_2^{mes})^2}{u_2^{mes2}} \right)$$

$$(2.162) \quad U_1 = \frac{F_1}{E} + u_{undef}$$

$$(2.163) \quad U_2 = \frac{F_2}{E} + u_{undef}$$

This cost function can be shown qualitatively as Figure 2.19. By having this function in the 3D medium, a good concept can be obtained. The sensitivity of the cost function concerning these parameters is different. So, the cost function is plotted concerning the dimensionless parameters as below:

$$(2.164) \quad J(\tilde{E}, \tilde{u}_{undef}) = \frac{1}{2u_1^2} \left(\frac{F_1^{mes}}{E} + u_{undef} - u_1^{mes} \right) + \frac{1}{2u_2^2} \left(\frac{F_2^{mes}}{E} + u_{undef} - u_2^{mes} \right)$$

Such that:

$$(2.165) \quad E = (1 + \tilde{E})\bar{E}$$

$$(2.166) \quad u_{undef} = (1 + \tilde{u}_{undef})\bar{u}_{undef}$$

The CMA code minimizes the mentioned J concerning the difference between the calculated and measured stiffness coefficient and calculated and measured undeformed length. The result is shown in the Figure 2.20

For solving the inverse problem for the material parameter and the unloaded configuration, the cost function has to parameters as Figure 2.19. This cost function has a different sensitivity to its variables. The sensitivity can be normalized by changing the variables:

$$(2.167) \quad E = (1 + \tilde{E})\bar{E}$$

$$(2.168) \quad u_{undef} = (1 + \tilde{u}_{undef})\bar{u}_{undef}$$

The two-dimensional minimization is shown from each intersection near the minimum configuration in Figure 2.19 and is compared with the results of the CMA code.

2.3.5.2 Rivlin Cube

Here we have the last two unknown parameters plus three new ones like λ_1 , λ_2 , and λ_3 . One data point is needed for estimating the unloaded configuration, and one more is needed for the material parameter estimation as the problem dimension is more than the material problem parameters. So our cost function has five unknowns. The difference between this part and section 1.4.2.2 in which the problem was only the material parameters; here, the cost function has five parameters to minimize. The result of minimization of the cost function with five data points is presented in Figure 2.21. In each graph, the cost function minimization is shown concerning the mentioned parameter.

$$(2.169) \quad J = \frac{1}{2} \left\{ \frac{[X_1 - X_1^{mes}]^2}{[X_1^{mes}]^2} + \frac{[X_2 - X_2^{mes}]^2}{[X_2^{mes}]^2} + \frac{[X_3 - X_3^{mes}]^2}{[X_3^{mes}]^2} + \frac{[X_4 - X_4^{mes}]^2}{[X_4^{mes}]^2} + \frac{[X_5 - X_5^{mes}]^2}{[X_5^{mes}]^2} \right\}$$

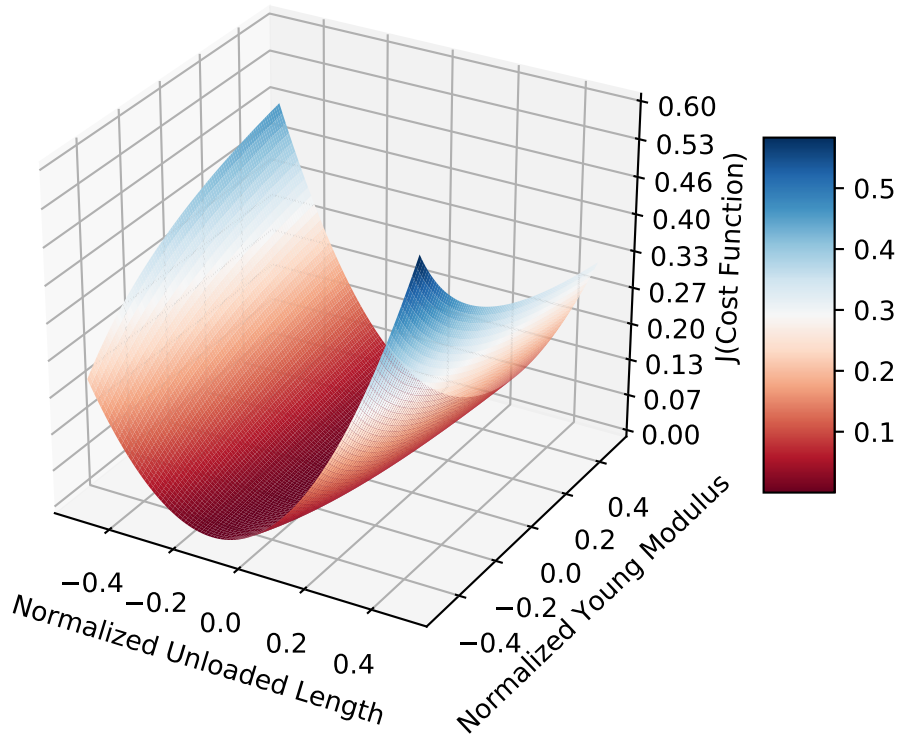


Figure 2.19: Linear spring cost function minimization with respect to the re-scaled parameters of the unloaded configuration and Young modulus

2.3.5.3 Tube

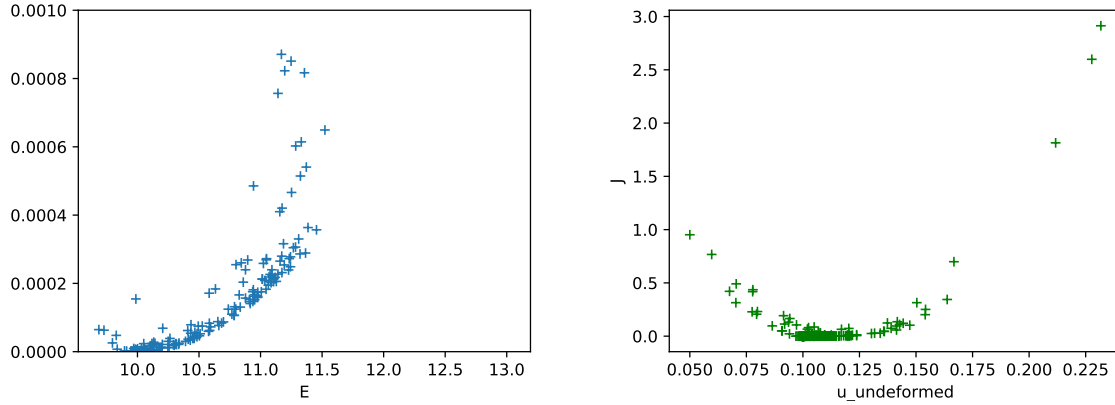
For the tube problem, the young modulus exists as the material parameter and the unloaded configuration. There are some time steps, which are the configurations of the tube for different values of the inner pressure. In Figure 2.2 the first and the last time step has been shown.

The tube studied here has a young modulus as its material parameter and n -dimensional coordinates. There are a side of material parameters and an aspect of the unloaded configuration in an inverse problem. For the unloaded configuration, each loaded measured configuration creates as many equations as it is needed to obtain the unloaded configuration.

The material parameter depends on the dimension of the problem. So, suppose the coordinates of the problem are more than the material parameters. In that case, one data point of the measured coordinates creates as many equations as needed to obtain the material parameters.

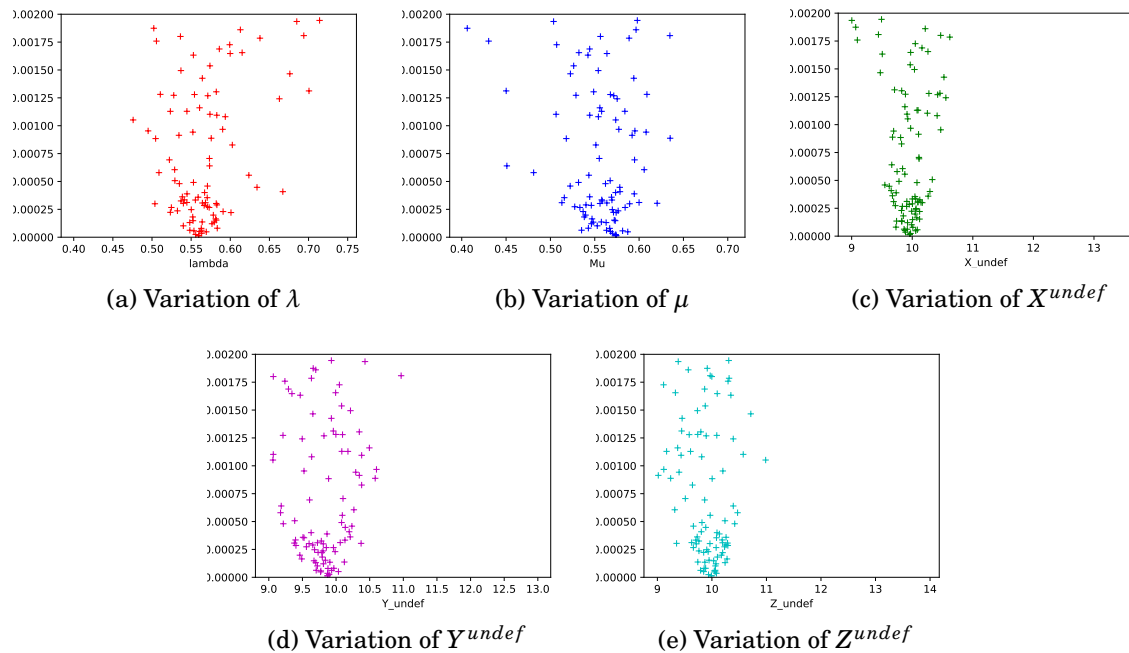
The unloaded configuration material parameter estimation for the tube has been solved with three different methods. These methods differ in the minimization of the cost function. The first

CHAPTER 2. COMBINED ESTIMATION OF MATERIAL PARAMETERS AND UNLOADED CONFIGURATIONS



(a) Minimization of the cost function with respect to E (b) Minimization of the cost function with respect to undeformed displacement

Figure 2.20: Minimization of the cost of the linear spring with respect to two parameters of the unloaded configuration and stiffness coefficient



(a) Variation of λ

(b) Variation of μ

(c) Variation of X^{undef}

(d) Variation of Y^{undef}

(e) Variation of Z^{undef}

Figure 2.21: Minimization of Mooney-Rivlin cube cost function with respect to re-scaled material parameters λ and μ and unloaded configuration parameters.

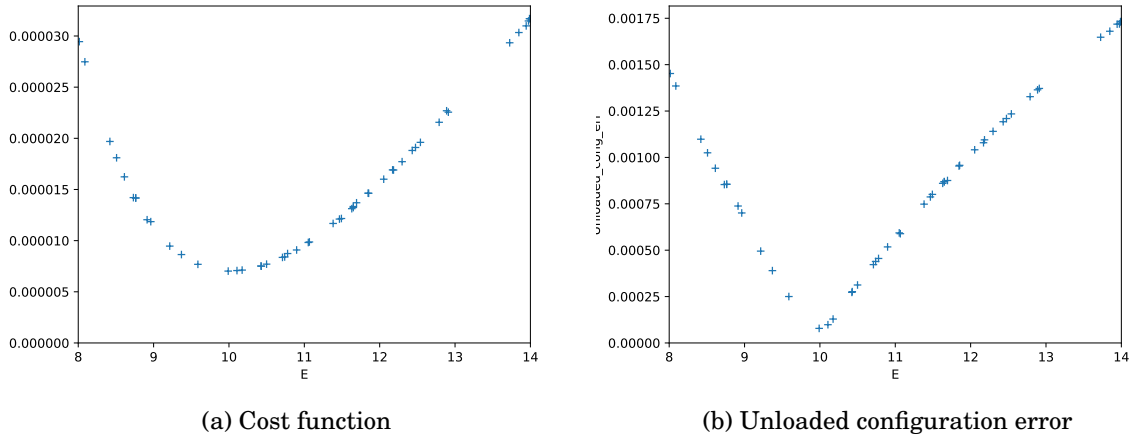


Figure 2.22: Tube cost function minimization for the unloaded configuration and material parameter estimation via CMA code.

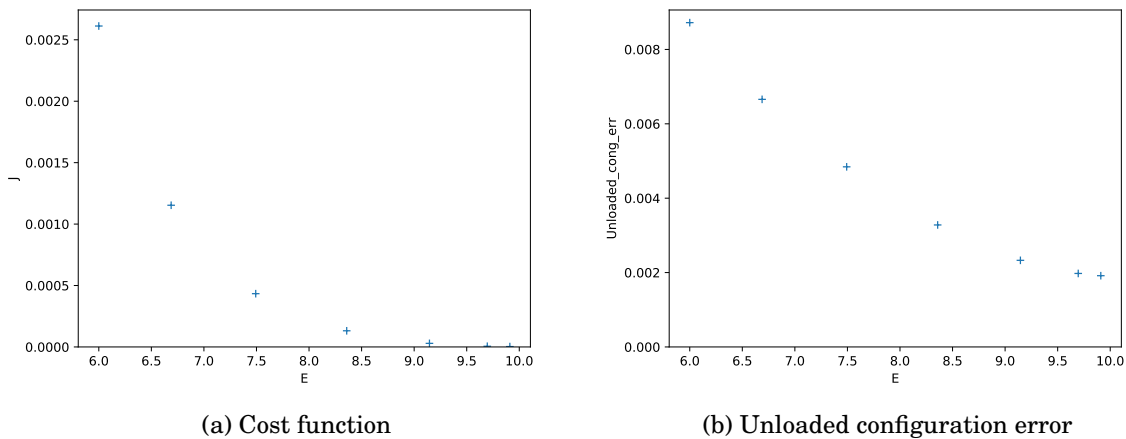


Figure 2.23: Tube cost function minimization for the unloaded configuration and material parameter estimation via Newton method.

model presented in Figure 2.22 is the least efficient one. This has been optimized with CMA code, and the minimization takes between 40 to 50 iterations.

Figure 2.23 and Figure 2.24 show the Newton solver for minimizing the cost function and Gradient Descent solver, respectively. These two methods take almost equal iterations to solve, and both around 10. It is needed to solve the inverse problem for Gradient Descent twice in each iteration and for Newton solver three times. So, the newton solver takes 1.5-time iterations of the Gradient Descent method. Notably, choosing the first step convergence coefficient γ_1 may also affect the overall steps.

The notable point about the Newton solver and Gradient Descent is that the error cannot be

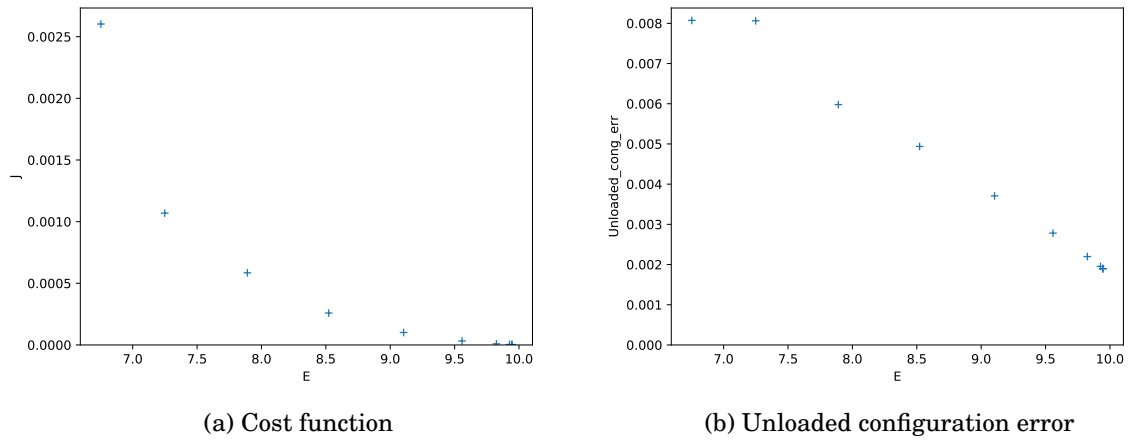


Figure 2.24: Tube cost function minimization for the unloaded configuration and material parameter estimation via gradient descent method.

smaller than a value. This fact is because of using numerical gradient. In these methods, there is the unloaded configuration error, and by choosing small values of h , the gradient can be affected by the error of the unloaded configuration tolerance.

2.4 Finite Differences Approximation of the Derivative and Hessian Matrix

2.4.1 Computing the Gradient of Some Functions

Here there are the numerical gradient and Hessian matrix of some cost functions near their minimum, which were used in the last sections, which are calculated with finite differences.

The cost functions defined before had as many as terms as unknown parameters. In the next section, the identifiability of the parameters is discussed. It is shown that for cost functions that had fewer terms as needed to identify parameters, the eigenvalues would not be positive, which means that the cost function does not have at that point.

2.4.1.1 Linear Spring

For minimizing the cost function for the linear spring with unknown unloaded configuration, Equation (2.161) was proposed. The young modulus and the unloaded configuration can be determined by minimizing the mentioned cost function. So, the gradient of mentioned cost function near the solution can be determined with a finite difference:

$$(2.170) \quad \underline{Grad}(J(E, u_{undef})) = \begin{bmatrix} -0.054 \\ 3.6 \end{bmatrix}$$

And Hessian matrix near this point:

$$(2.171) \quad \underline{\underline{H}}(J(E, u_{undef})) = \begin{bmatrix} 0.109 & -0.060 \\ -0.060 & 4.0 \end{bmatrix}$$

The Hessian matrix eigenvalues are 0.108 and 4.0, which are positive, which means that the function has a minimum in the solution neighborhood. If the cost function be assumed as equation (2.172)

$$(2.172) \quad J(E, u_{undef}) = \frac{1}{2} \frac{(U_1 - u_1^{mes})^2}{u_1^{mes2}}$$

There is one less data point than it is needed to determine all the parameters needed. So, probably the cost function would not have a minimum near the solution. In this condition, the Hessian matrix would be as equation 2.173

$$(2.173) \quad \underline{\underline{H}}(J(E, u_{undef})) = \begin{bmatrix} 0.036 & -0.020 \\ -0.020 & 2.0 \end{bmatrix}$$

For the mentioned Hessian matrix, eigenvalues would be -0.018 and 1.8, which means that the function does not have a minimum near the solution.

2.4.1.2 Non-linear Spring

The cost function for determining the unloaded configuration and two material parameters for the non-linear spring, as discussed before is as below:

$$(2.174) \quad J(E_0, \epsilon_1, u_{undef}) = \frac{1}{2} \left(\frac{(U_1 - u_1^{mes})^2}{u_1^{mes2}} + \frac{(U_2 - u_2^{mes})^2}{u_2^{mes2}} + \frac{(U_3 - u_3^{mes})^2}{u_3^{mes2}} \right)$$

The young modulus and the unloaded configuration can be determined by minimizing the mentioned cost function. So, the gradient of the mentioned cost function near the solution can be determined with a finite difference:

$$(2.175) \quad \underline{\underline{Grad}}(J(E_0, \epsilon_1, u_{undef})) = \begin{bmatrix} 3.00 * 10^{-6} \\ 3.87 * 10^{-5} \\ 3.22 * 10^{-7} \end{bmatrix}$$

And Hessian matrix near this point:

$$(2.176) \quad \underline{\underline{H}}(J(E, u_{undef})) = \begin{bmatrix} 6. & -19.0 & -1.70 \\ -19.0 & 77.50 & 3.85 \\ -1.70 & 3.85 & 0.64 \end{bmatrix}$$

The eigenvalues of the Hessian matrix are 82.44, 1.68 and 0.00208 which are positive and this means that the function has a minimum in the neighborhood of the solution.

If the cost function is assumed as below:

$$(2.177) \quad J(E_0, \epsilon_1, u_{undef}) = \frac{1}{2} \left(\frac{(U_1 - u_1^{mes})^2}{u_1^{mes2}} + \frac{(U_2 - u_2^{mes})^2}{u_2^{mes2}} \right)$$

There is one less data point than it is needed to determine all the parameters needed. So, probably the cost function would not have a minimum near the solution. In this condition, the Hessian matrix would be as below.

$$(2.178) \quad \underline{\underline{H}}(J(E_0, \epsilon_1, u_{undef})) = \begin{bmatrix} 2.0 & -11 & -0.2 \\ -11 & 60.50 & 1.10 \\ -0.2 & 1.1 & 0.02 \end{bmatrix}$$

For the mentioned Hessian matrix, eigenvalues would be 62.5, $1.37 * 10^{-5}$, and $-1.94 * 10^{-7}$, which means that the function does not have a minimum near the solution.

2.4.1.3 Rivlin Cube

The cost function for determining the unloaded configuration and two material parameters μ and λ for the non-linear spring, as discussed before, is as below:

$$(2.179) \quad J(\mu, \lambda) = \frac{1}{2} \left(\frac{(X_1(0) - X_1(0)^{mes})^2}{X_1(0)^{mes2}} + \frac{(X_1(1) - X_1(1)^{mes})^2}{X_1(1)^{mes2}} \right)$$

μ and λ can be determined by minimizing the mentioned cost function. So, the gradient of the mentioned cost function near the solution can be determined with a finite difference:

$$(2.180) \quad \underline{\underline{Grad}}(J(\mu, \lambda)) = \begin{bmatrix} 8.81 * 10^{-9} \\ 3.81 * 10^{-7} \end{bmatrix}$$

And Hessian matrix near this point:

$$(2.181) \quad \underline{\underline{H}}(J(\mu, \lambda)) = \begin{bmatrix} 0.018 & -0.072 \\ -0.072 & 0.76 \end{bmatrix}$$

The eigenvalues of the Hessian matrix are 0.0107 and 0.769 which are positive, and this means that the function has a minimum in the neighborhood of the solution.

If the cost function is assumed as below:

$$(2.182) \quad J(\mu, \lambda) = \frac{1}{2} \left(\frac{(X_1(0) - X_1(0)^{mes})^2}{X_1(0)^{mes2}} \right)$$

2.4. FINITE DIFFERENCES APPROXIMATION OF THE DERIVATIVE AND HESSIAN MATRIX

There is one less data point than is needed to determine all the parameters needed. So, probably the cost function would not have a minimum near the solution. In this condition, the Hessian matrix would be as below.

$$(2.183) \quad \underline{\underline{H}}(J(\mu, \lambda)) = \begin{bmatrix} 0.001 & 0.017 \\ 0.017 & 0.27 \end{bmatrix}$$

For the mentioned Hessian matrix, eigenvalues would be $-2.73 * 10^{-1}$ and $-3.11 * 10^{-9}$, which means that the function does not have a minimum near the solution.

LUNG MECHANICAL MODELING

3.1 Introduction

This section is more applied compared to what has been discussed before. There are some steps for modeling the lung and thorax and obtaining the displacement field between the exhalation and inhalation processes. The problem's input is the CT images of a person during the patient's inhalation and exhalation process. By these images, a 3D model can be simulated.

3.1.1 Lung Mesh

For starting this procedure, we would need some raw data. There are two sets of data: the raw CT images captured from the patients in the respiration process and the mask images obtained from the mentioned images.

This step should be done by MeVisLab software, where we insert the raw images plus the mask images, which should become inverse and modify to be compatible with the CT images. By doing so, lung surface mesh would be available as Figure 3.1.

The image mentioned above is the lung surface mesh, which needed to be transformed into a 3D mesh with which it is possible to extract the nodes' displacement field. The 3D mesh will be achieved by GMSH software. Furthermore, in the end, a 3D mesh as Figure 3.2 is available.

3.1.2 Thorax Mesh

The same process should be done for the thorax, but it is different from the lung mesh. For the thorax surface mesh, contours should be inserted in the CT images, and by processing it in MeVisLab, the 3D mesh would be created. Contours created in MeVisLab are shown in Figure 3.3.

The surface mesh obtained from the GMSH software is Figure 3.4

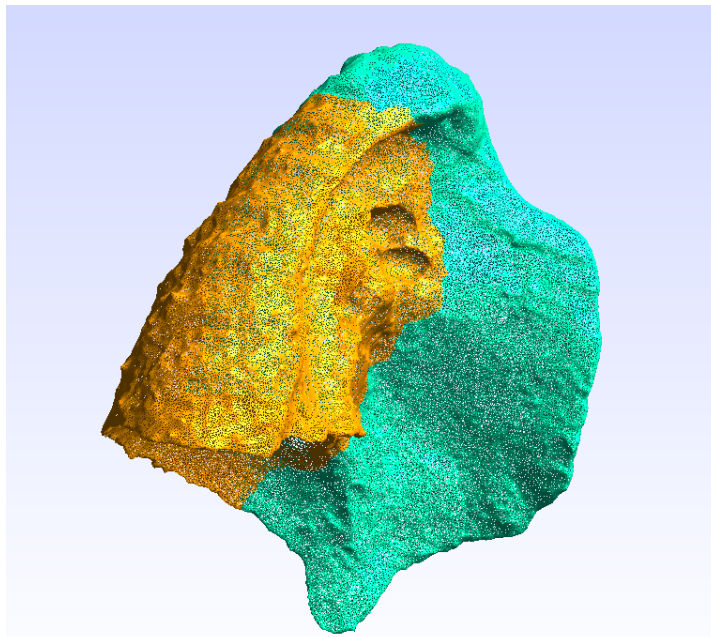


Figure 3.1: Lung surface mesh obtained in MeVisLab

The same process would be repeated for obtaining the 3D mesh, and Figure 3.5 shows the 3D mesh created by GMSH.

3.1.3 Lung Porosity

One of the steps to find the lung displacement field from exhalation to inhalation is finding the lung porosity, as the lung contains air and blood as fluid. This needs a two-step process; one is done with Matlab and the other with Python.

The Matlab code's output is an image with the ".vtk" format, which needed to be changed to a ".vti" format that occupies less space, and this would be done by Paraview software. In Figure 3.6 you can use a raw CT image and an image by considering the porosity.

This step's importance is when the lung's stiffness is needed, and it is evident that the lung is not a uniform material, and there is porosity on it. As it is shown in Figure 3.6.

3.1.4 Thorax Displacement Field

We have the thorax mesh at the end of the exhalation and the end of the inhalation. What is interesting here is how the thorax would deform between these two-time steps. First, the mask images of the thorax with the output images of the MeVisLab and a developed code in Python; the result would be a set of images with red color in the thorax area and blue color at rest as Figure 3.8

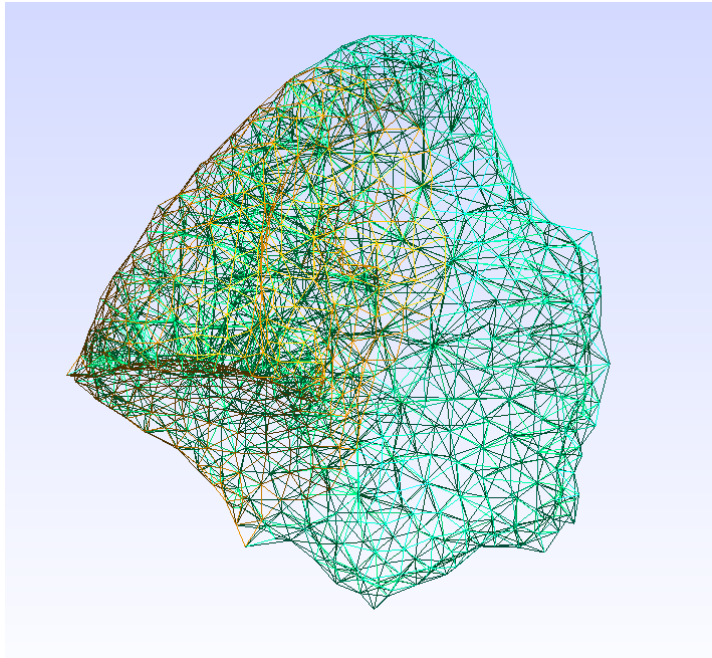


Figure 3.2: Lung 3D mesh obtained in GMSH from the surface mesh

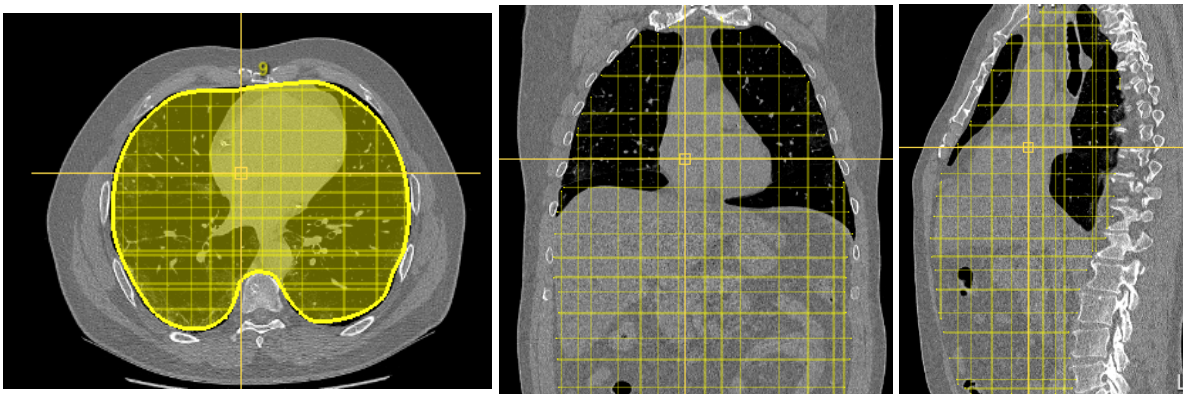


Figure 3.3: Lung CT images in three different angles

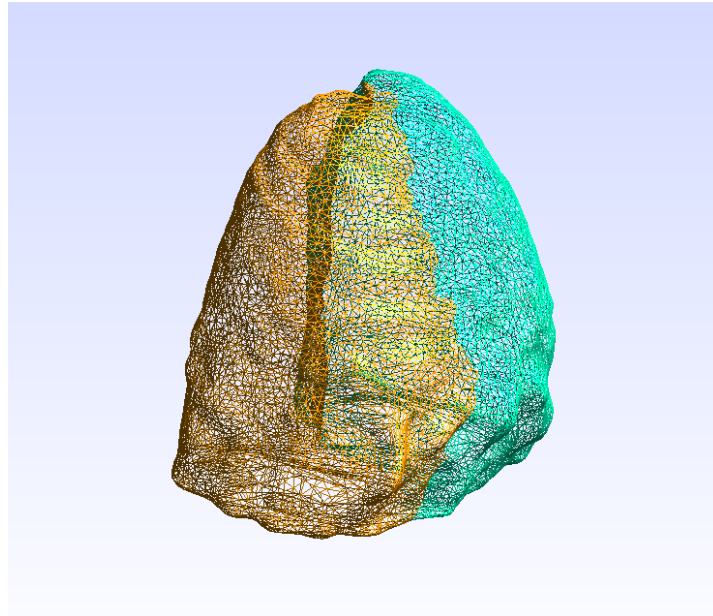


Figure 3.4: Thorax surface mesh obtained in MeVisLab

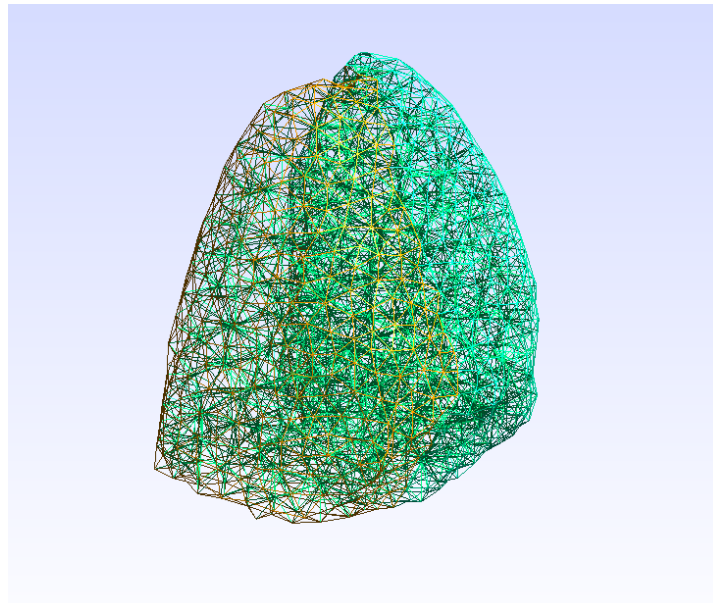


Figure 3.5: Thorax 3D mesh obtained in GMSH

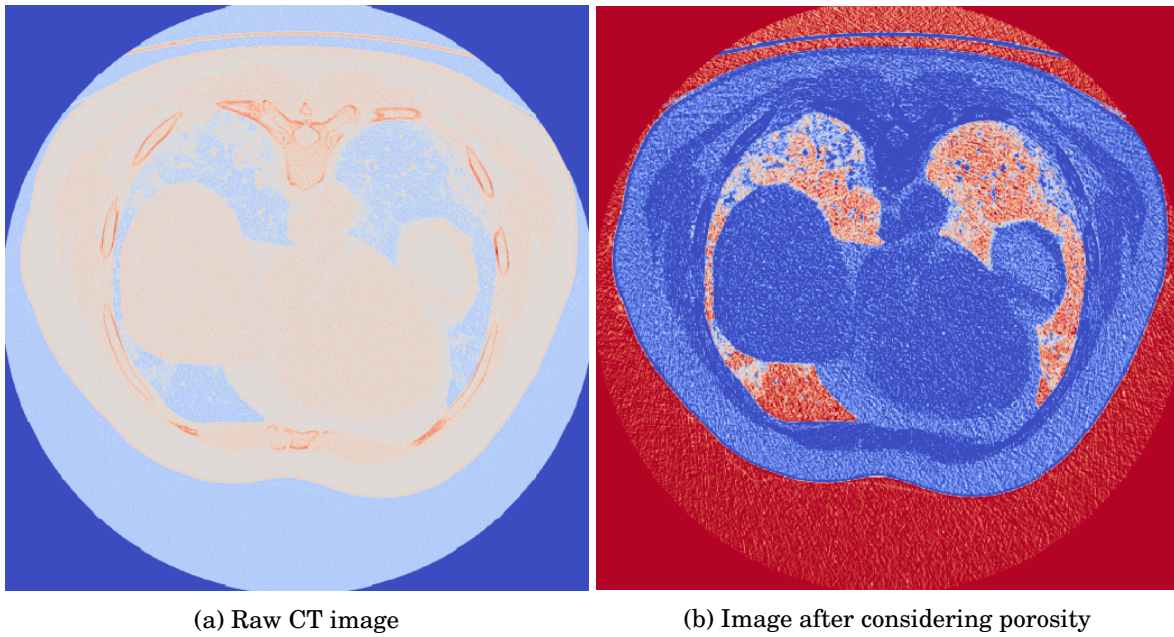


Figure 3.6: CT image before and after porosity consideration

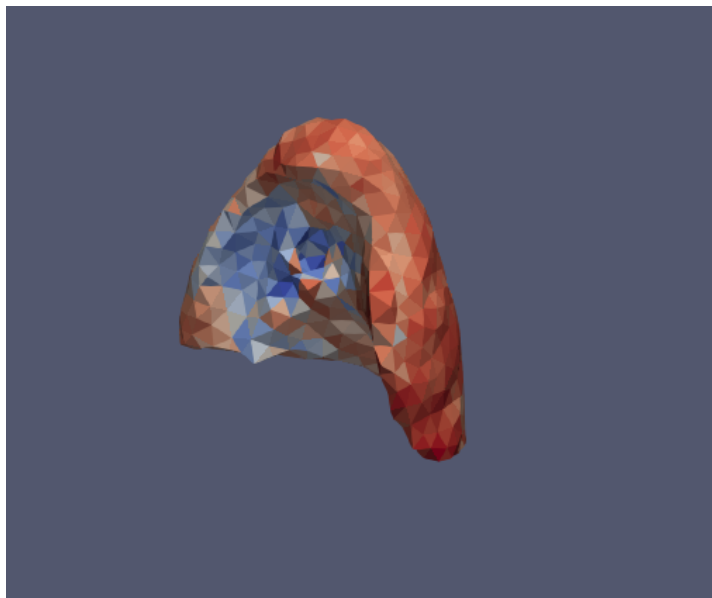
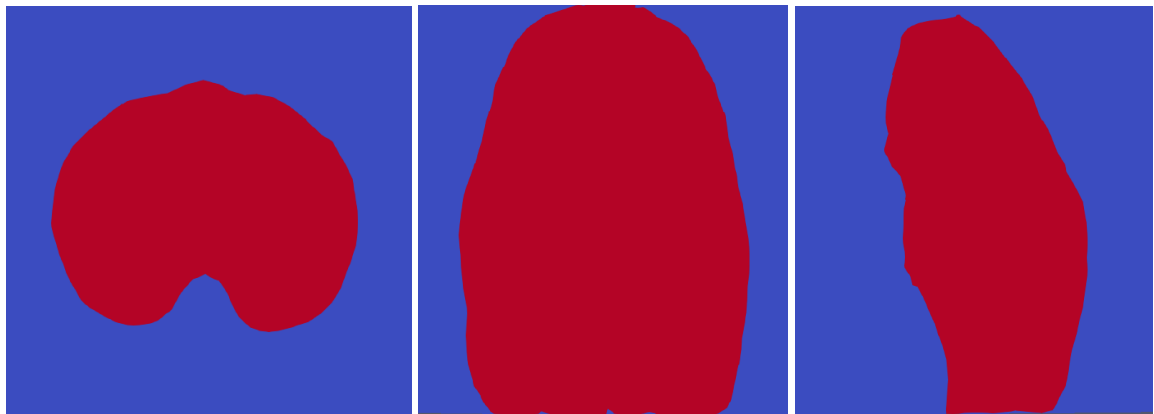
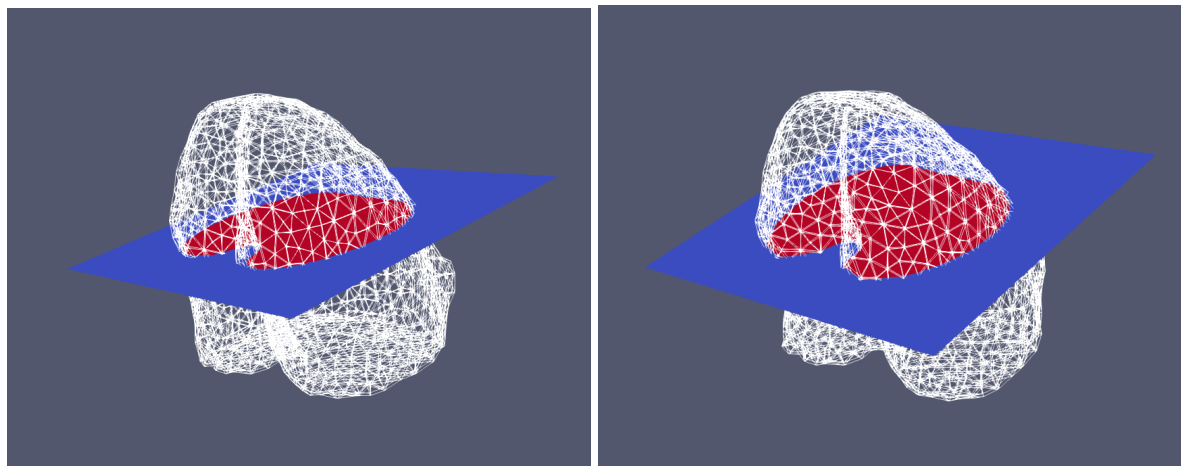


Figure 3.7: The right lung with different values of porosity. Blue color shows zero porosity and red color show parts with porosity equal to one.



(a) Thorax mask image in the XY plane (b) Thorax mask image in the XZ plane (c) Thorax mask image in the YZ plane

Figure 3.8: Thorax mask images in three different angles



(a) Thorax mesh at the end of exhalation

(b) Thorax mesh at the end of inhalation

Figure 3.9: Thorax displacement field from end of the exhalation process and end of the inhalation process

DISCUSSION AND ONGOING RESEARCH

There are two classical problems in biomechanics; one is estimating the unloaded configuration of the problems in which only the loaded configuration and the loaded pressure is known, and the other one is the kind of problems in which the unloaded configuration is known beside the loaded configuration and applied force, but the material parameters are not known.

The uniqueness of our work is by combining the two above problems. It means that for problems in which neither the unloaded configuration nor the material parameters are known, both can be estimated if there are enough data points in the form of loaded configuration with corresponded applied force.

The combined estimation of unloaded configuration and material parameter estimation needs a few data points in different models. The golden point is that for estimating the unloaded configuration, one data point is enough as it can produce as many as equation as is needed for finding the unloaded configuration, and there is one data point for the material parameter estimation if the dimension of the problem is more than the number of material parameters.

To continue this research, some steps can be improved in optimization. One is using statistical tools for finding the global minimum of a specific cost function. Another one is regarding the gradient of the cost function. In this research, the gradient has been obtained numerically via finite-difference. Nevertheless, the goal of and following research is to obtain the gradient by solving the adjoint problem.

BIBLIOGRAPHY

- [1] S. AVRIL, M. BONNET, A.-S. BRETTELLE, M. GRÉDIAC, F. HILD, P. IENNY, F. LATOURTE, D. LEMOSSE, S. PAGANO, E. PAGNACCO, AND F. PIERRON, *Overview of Identification Methods of Mechanical Parameters Based on Full-field Measurements*, *Experimental Mechanics*, 48 (2008), pp. 381–402.
- [2] M. BONNET AND A. CONSTANTINESCU, *Inverse problems in elasticity*, *Inverse Problems*, 21 (2005), pp. R1–R50.
- [3] M. GENET, M. RAUSCH, L. LEE, S. CHOY, X. ZHAO, G. KASSAB, S. KOZERKE, J. GUCCIONE, AND E. KUHL, *Heterogeneous growth-induced prestrain in the heart*, *Journal of Biomechanics*, 48 (2015), pp. 2080–2089.
- [4] M. GENET, C. STOECK, C. VON DEUSTER, L. LEE, AND S. KOZERKE, *Equilibrated warping: Finite element image registration with finite strain equilibrium gap regularization*, *Medical Image Analysis*, 50 (2018), pp. 1–22.
- [5] M. GENET, C. T. STOECK, C. VON DEUSTER, L. C. LEE, J. GUCCIONE, AND S. KOZERKE, *Finite element digital image correlation for cardiac strain analysis from 3d whole-heart tagging*, *Journal of Biomechanics*, 58 (2016).
- [6] S. GOVINDJEE AND P. A. MIHALIC, *Computational methods for inverse finite elastostatics*, *Computer Methods in Applied Mechanics and Engineering*, 136 (1996), pp. 47–57.
- [7] S. GOVINDJEE AND P. A. MIHALIC, *Computational methods for inverse deformations in quasi-incompressible finite elasticity*, (1998), p. 18.
- [8] C. PATTE, D. CHAPELLE, AND M. GENET, *Estimation of patient-specific mechanical parameters in pulmonary diseases*.
- [9] C. PATTE, M. GENET, AND D. CHAPELLE, *A poromechanical model of the lungs*.
- [10] C. 'E. C. PATTE, M. GENET, C. FETITA, P.-Y. BRILLET, AND D. CHAPELLE, *Personalized pulmonary mechanics: modeling and estimation - application 'pulmonary fibrosis*, *Journal of Biomechanics*, v1 (2019).

BIBLIOGRAPHY

- [11] M. K. RAUSCH, M. GENET, AND J. D. HUMPHREY, *An augmented iterative method for identifying a stress-free reference configuration in image-based biomechanical modeling*, *Journal of Biomechanics*, 58 (2017), pp. 227–231.
- [12] M. SELLIER, *An iterative method for the inverse elasto-static problem*, *Journal of Fluids and Structures*, 27 (2011), pp. 1461–1470.